Annex NanoOnSpect – Final publishable summary report

Figures and tables

1. Executive summary

2. Summary description of project context and main objectives

3. Description of project context and main S&T results / foregrounds

3.1 WP1 Online nanocomposite characterization device

3.1.1 Main objectives

3.1.2 Pressure and temperature sensing

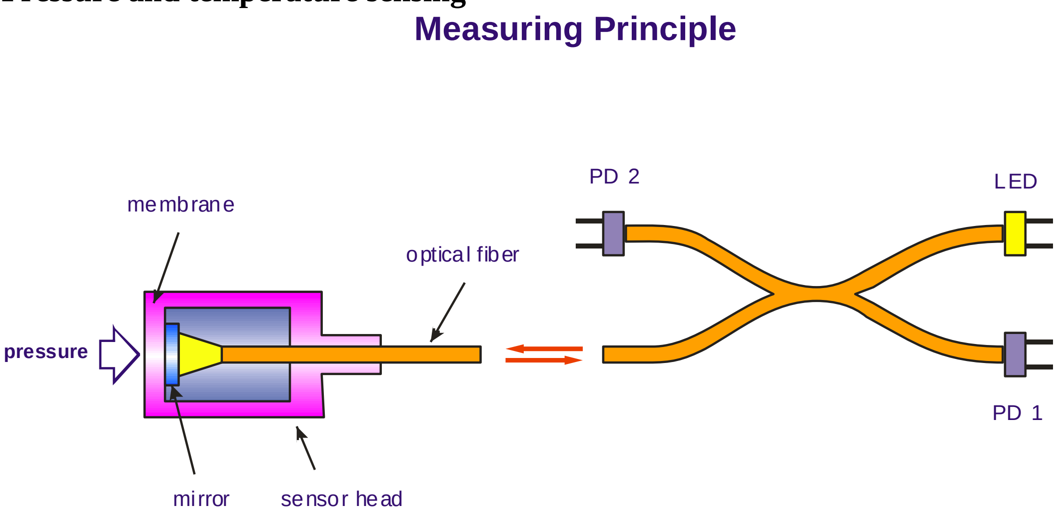

Figure 3.1.2.1: FOS measuring principle of the fiberoptical pressure sensor.

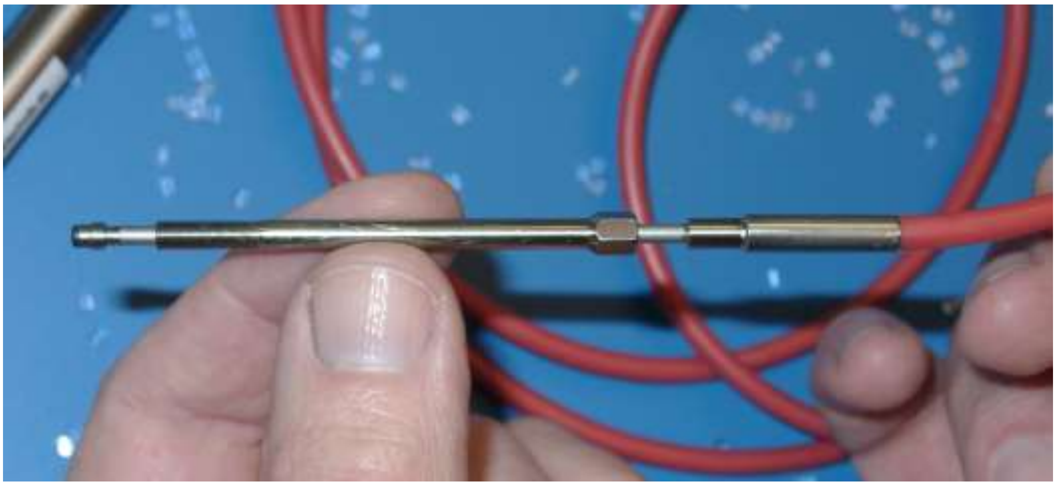

Figure 3.1.2.2: FOS miniature fiberoptical pressure sensor with Ø 3 mm frontend.

Figure 3.1.2.3: FOS IR-Melt-Thermometer with amplifier unit.

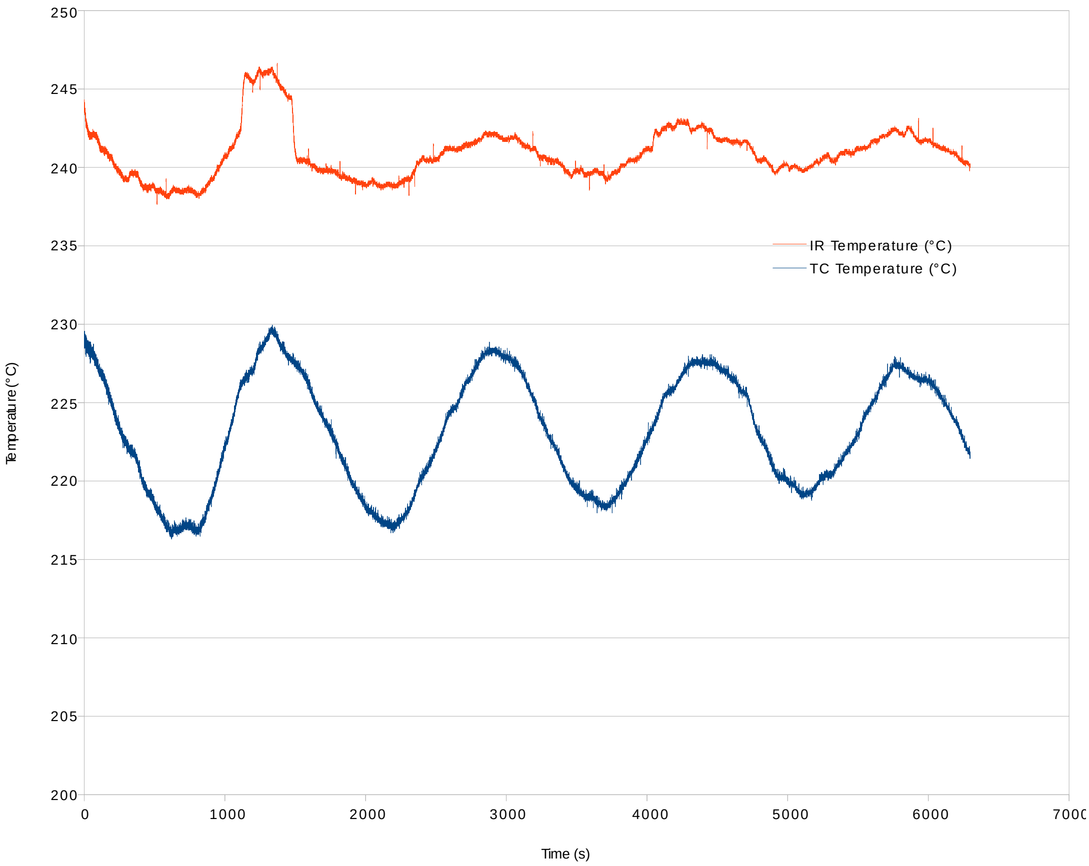

Figure 3.1.2.4: FOS IR-Melt-Thermometer signal readout during a test run. Red line = IR-Temperature signal. Blue line = Sensor head and extruder case temperature (thermocouple).

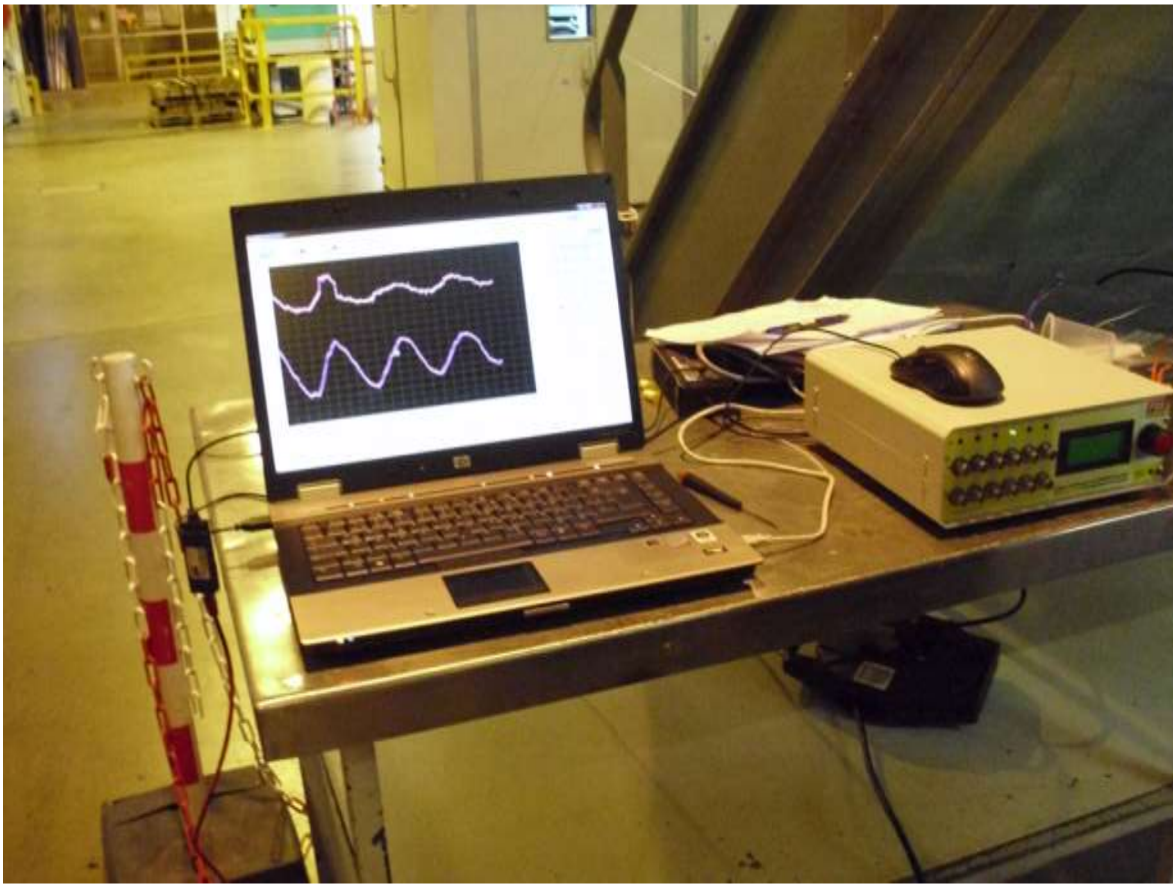

Figure 3.1.2.5: FOS IR-Melt-Thermometer signal readout during a test run. Upper line = IR-Temperature signal. Lower line = Sensor head and extruder case temperature (thermocouple). The step in the upper line was caused by a sudden change of screw speed.

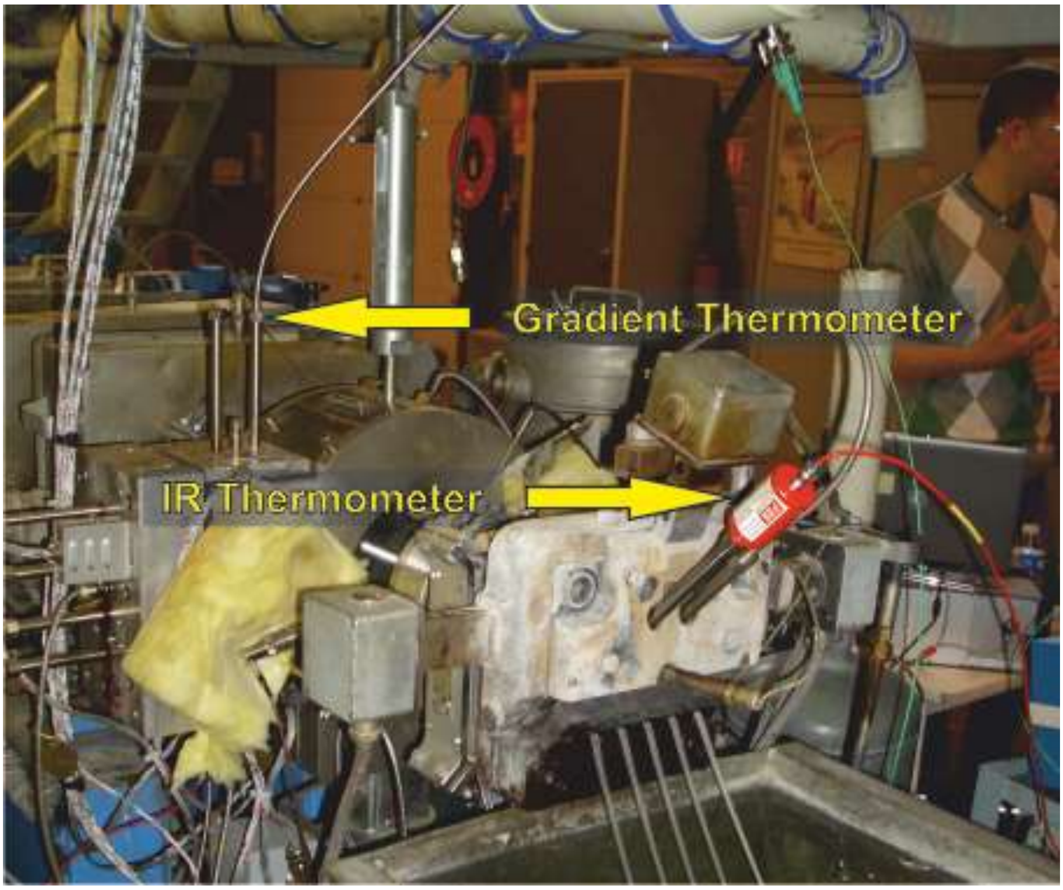

Figure 3.1.2.6: FOS IR-Melt-Thermometer mounted at an extruder head during test runs.

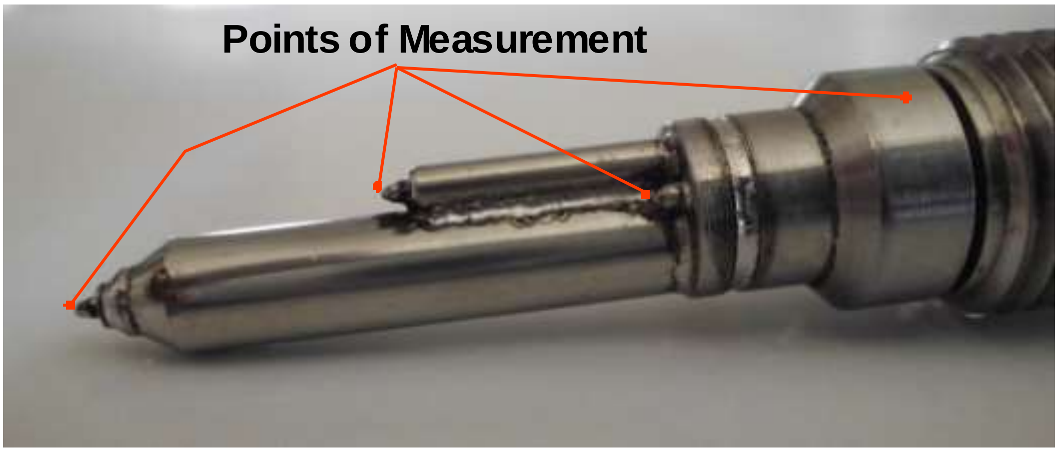

Figure 3.1.2.7: FOS multi point gradient thermometer frontend.

Figure 3.1.2.8: FOS multi point gradient thermometer measuring setup.

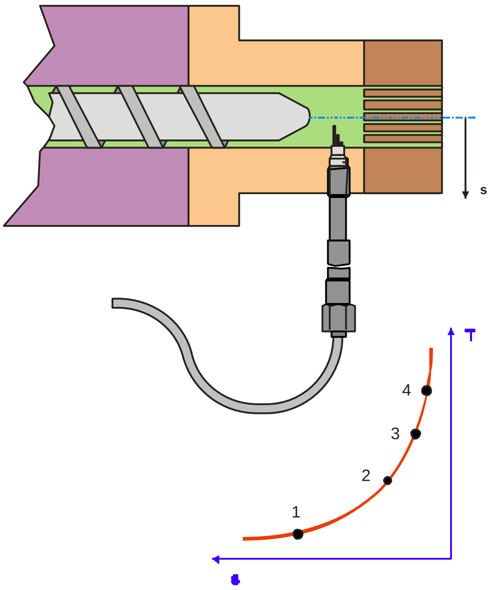

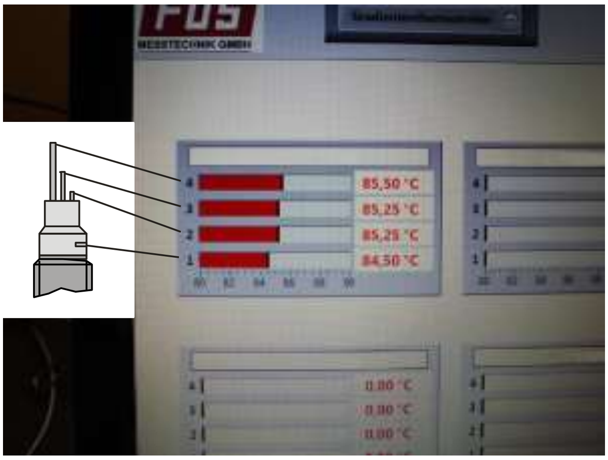

Screen Shot LabVIEW™ DAQ Software

Figure 3.1.2.9: FOS multi point gradient thermometer mounted at an extruder nozzle with signal display and temperature profile diagram.

3.1.3 Thermal conductivity sensing system

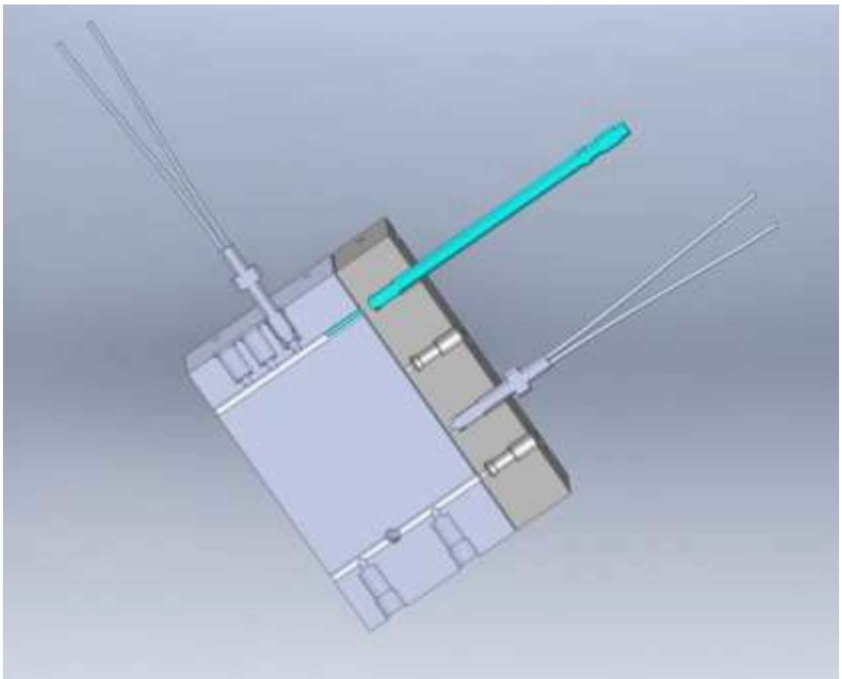

Figure 3.1.3.1: The prototype phase: ONBOX with two concepts of thermal needle: model NOS01 in blue/green; a needle in the melt flow. Two pieces of model NOS03, flush with the surface of the channels in the ONBOX. Model NOS03, although more robust did not attain the necessary sensitivity and reproducibility.

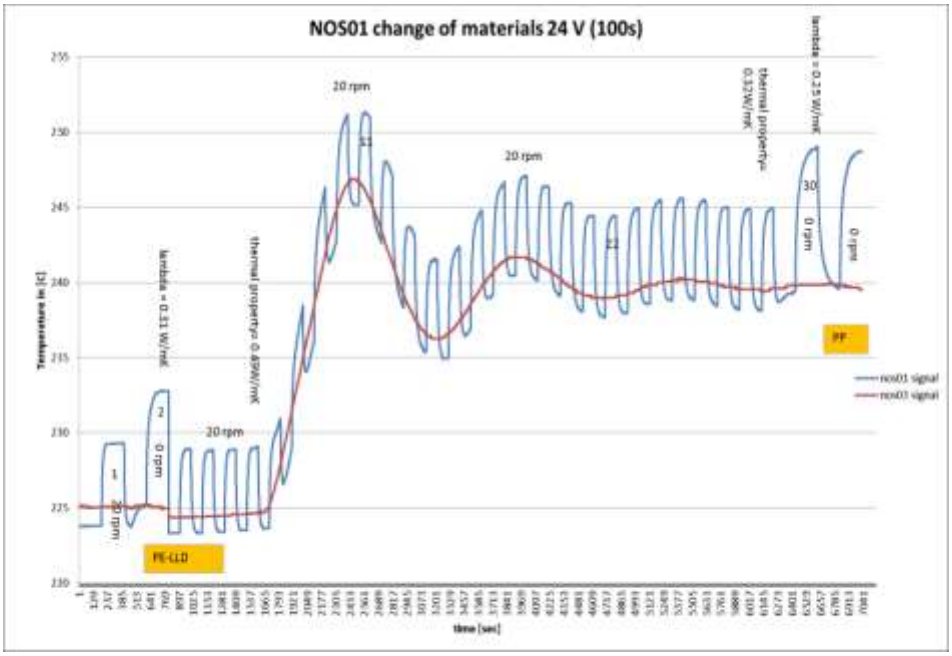

Figure 3.1.3.2: Example of experiments carried out for performance verification of NOS01. Experiments were carried out at different melt flows, expressed in rotations per minute, rpm,of the ONBOX pump/extruder, and with different plastics PE and PP. The ideal experiment for absolute thermal conductivity measurement takes place under static conditions, at 0 rpm. In case of flowing melt, at > 0 rpm, the measurements show an error; it is no longer possible to perform absolute measurements and only comparative measurements or monitoring of trends is possible.

Figure 3.1.3.3: Measurements at Gneuss on a real ONBOX in March 2012 on prototype sensors and measurement and control unit. The measurement and control in this phase are still autonomous.

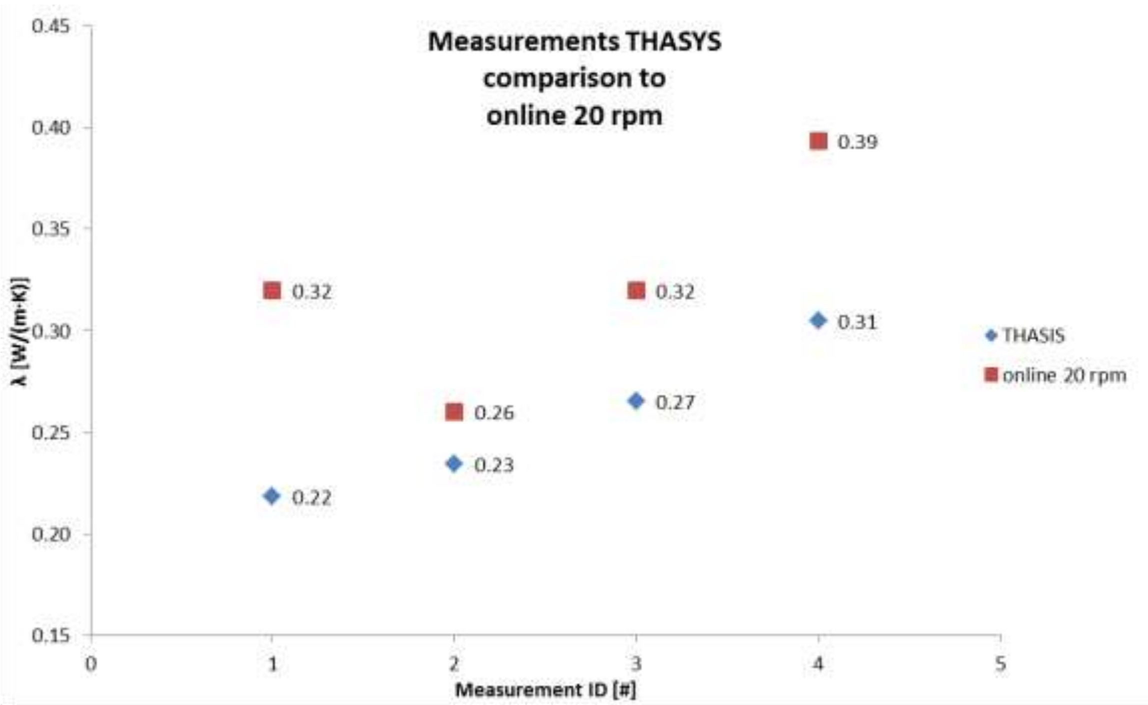

Figure 3.1.3.4: Melt properties and room temperature properties do no correlate. Blue squares are room temperature measurements on the solid plastic material on the THASYS system. Red squares are measurements performed on the melt at 20 rpm with NOS01. Results obtained in cooperation with AIMPLAS, who operated the extruder with ONBOX and made the solid specimens.

3.1.4 Rheology sensing system by capillary rheology

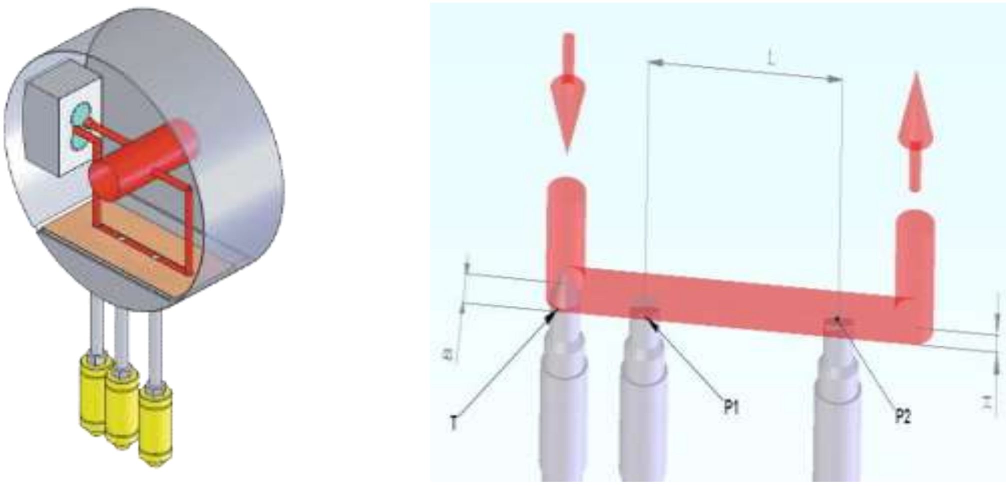

Figure 3.1.4.1. Basic design of rheology sensing unit and measurement principle

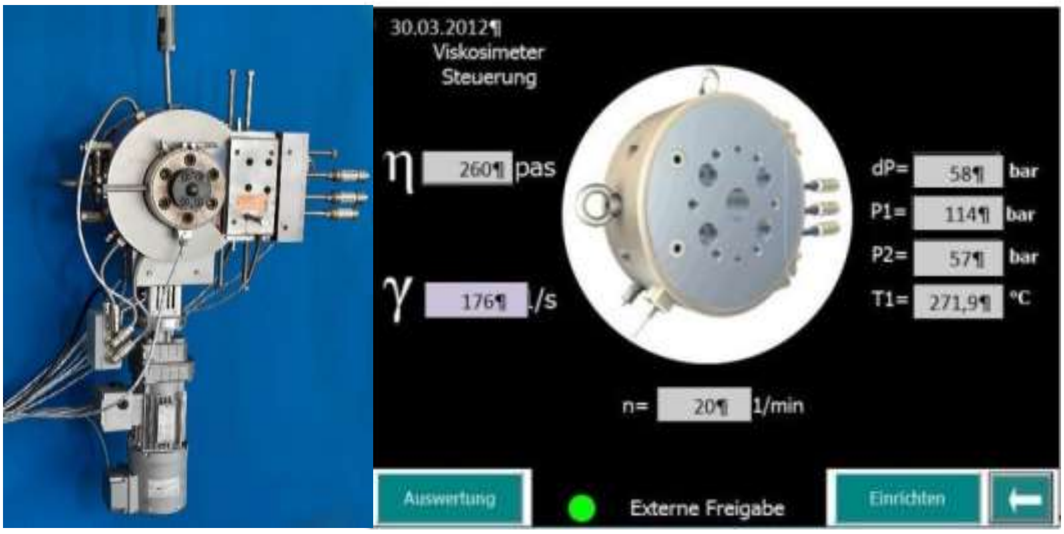

Figure 3.1.4.2: Prototype system and HMI Interface screenshot

3.1.5 Optical spectroscopy sensing system

Table 3.1.5.1: Legend equation (1)

I_R	Raman intensity
I_L	laser intensity
σ	Raman scattering cross-section
K	measuring parameter
P	path length
C	concentration

Table 3.1.5.2: The vibrational spectra of PP/MWCNTs (δ- bending; r- rocking; ν-streching; t-twisting; w- wagging)

	Schwingungsart	**Raman-Shift**
1	Al_2O_3 –Peak	415 cm^{-1}
2	Al_2O_3 –Peak	447 cm^{-1}
3	Al_2O_3 –Peak	577 cm^{-1}
4	Al_2O_3 -Peak	748 cm^{-1}
5	ν(C-C), r(CH_2) of PP	833 cm^{-1}
6	r(CH_3), ν(C-C) of PP	969 cm^{-1}
7	PP-Peak	1017 cm^{-1}
8	ν(C-C), δ(CH) of PP	1150 cm^{-1}
9	D-Peak of CNTS	1310 cm^{-1}
10	δ [-CH_2-] of PP	1460 cm^{-1}
11	G-Peak of CNTS	1605 cm^{-1}

Equation. 3.1.5.1

$I_R=(I_L \bullet \sigma \bullet K) \bullet P \bullet C$ (Eq. 3.1.5.1)

Equation. 3.1.5.1

$I=I_0 \bullet e^{(\varepsilon(\lambda) \bullet c \bullet d)}$ (Eq. 3.1.5.2)

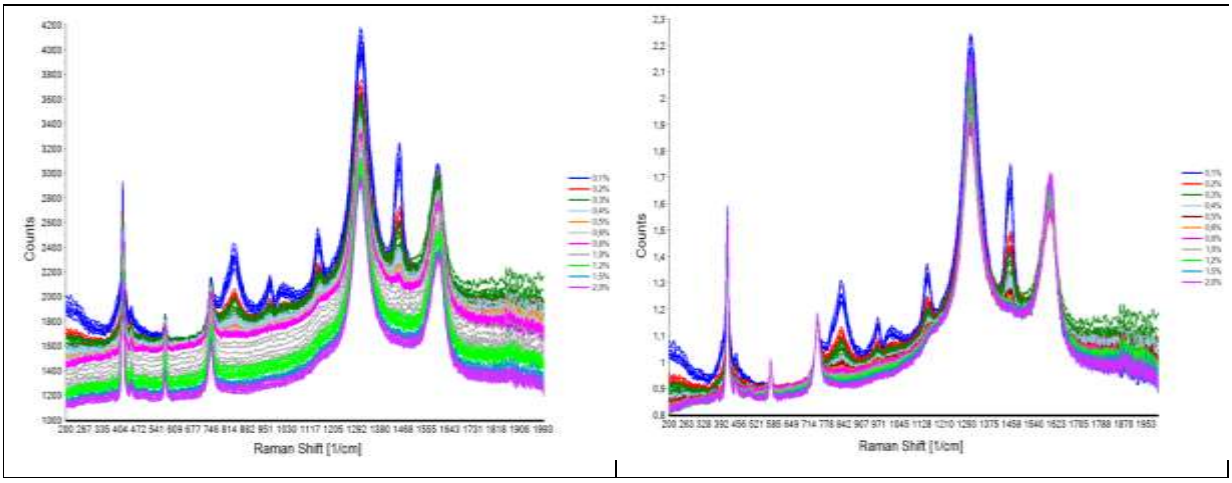

Figure 3.1.5.1: a) Raw spectra b) normalized spectra of pp/CNTs-composites containing 0.1%; 0.2%; 0.3%; 0.4%; 0.5%; 0.6%; 0.8%; 1.0%; 1.2%; 1.5% and 2% CNTs.

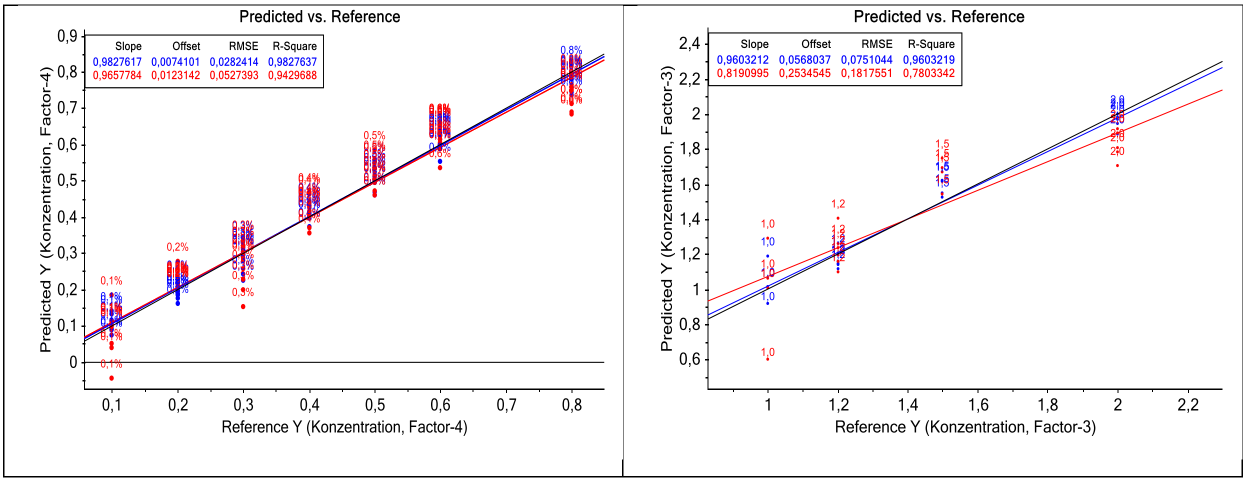

Figure 3.1.5.2: a) PLS multivariate calibration model with 4 PLS factors for the CNTs concentration range between 0.1 to 0.8 percent. b) PLS multivariate calibration model with 2 PLS factors for CNTs concentration range between 1 to 2 percent.

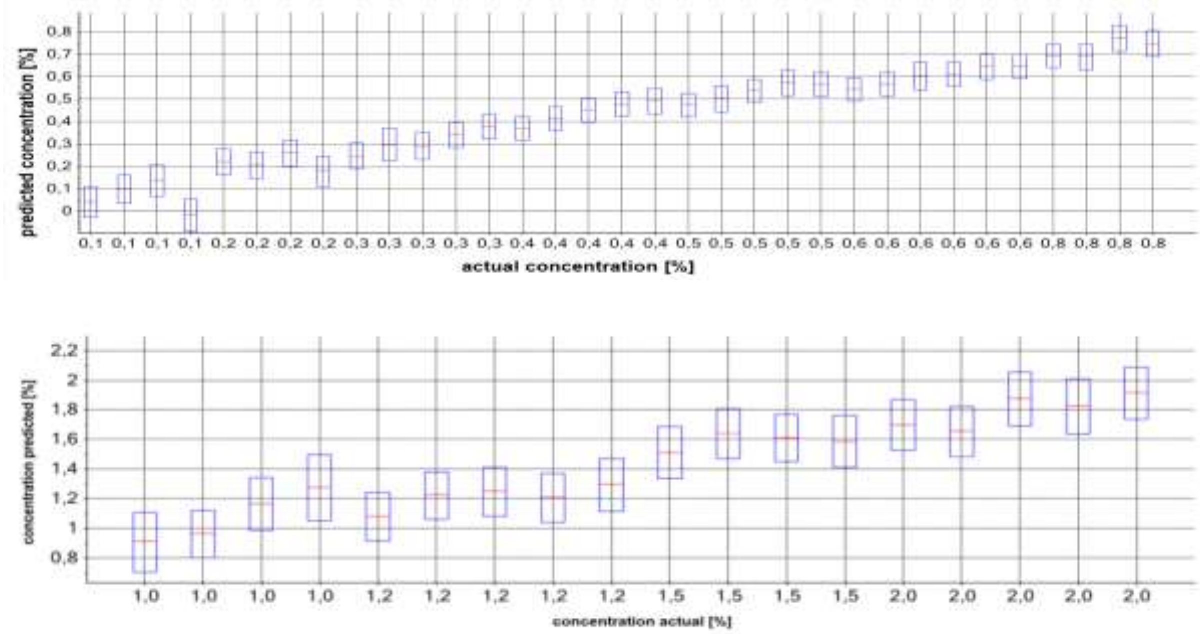

Figure 3.1.5.3: Results of the multivariate analysis of Raman spectra for the determination of the CNTS concentration. The plot shows predicted with error bar vs. actual concentration. a) CNTs concentration range between 0.1 to 0.8 percent. b) CNTs concentration range between 1 to 2 percent.

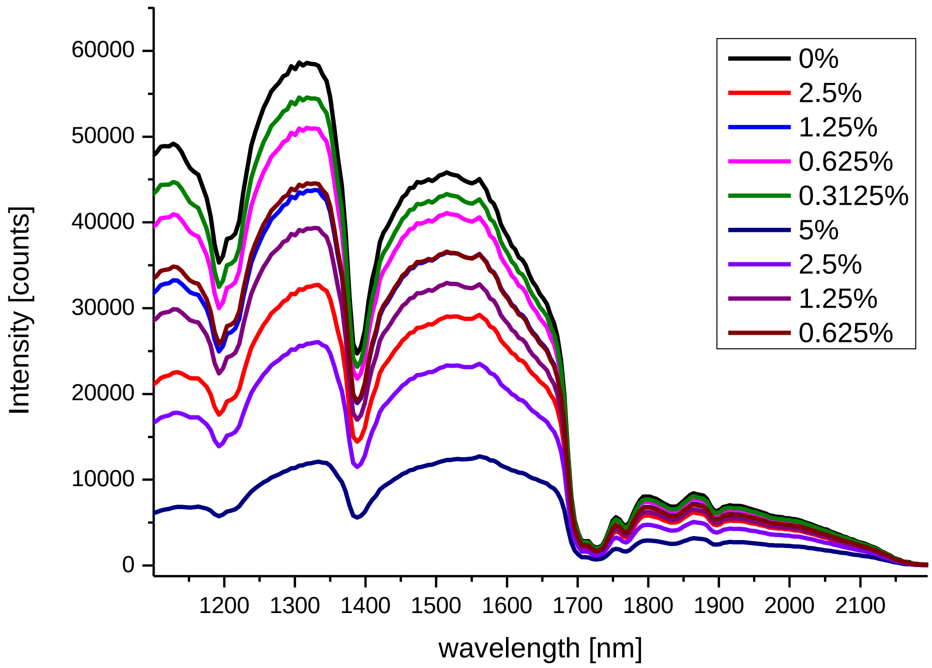

Figure 3.1.5. 4: NIR energy spectra pf PP/clay samples

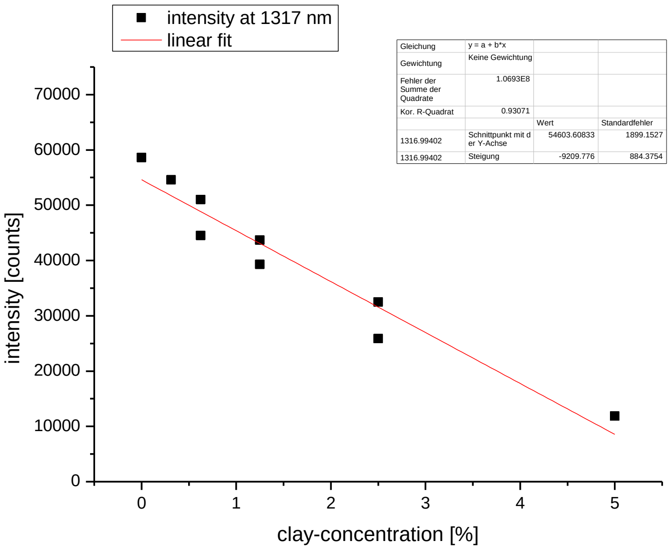

Gleichung	y = a + b*x		
Gewichtung	Keine Gewichtung		
Fehler der Summe der Quadrate	1.0693E8		
Kor. R-Quadrat	0.93071		
		Wert	Standardfehler
1316.99402	Schnittpunkt mit der Y-Achse	54603.60833	1899.1527
1316.99402	Steigung	-9209.776	884.3754

Figure 3.1.5.5: linear regression model for determination of the total content of clays at λ=1317nm

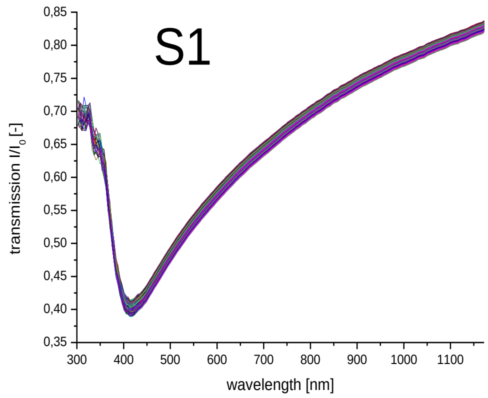

a) transmission spectra of sample S-1

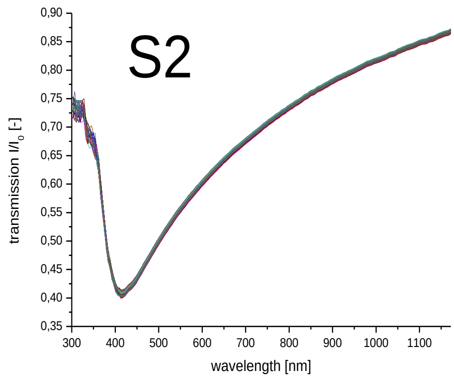

b) transmission spectra of sample S-2

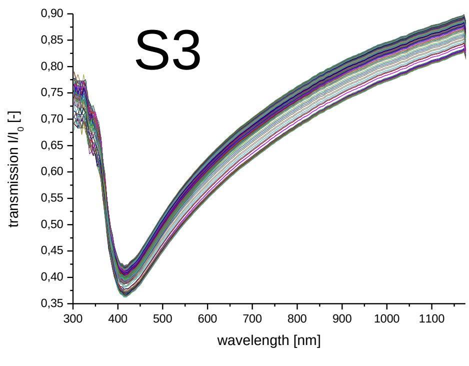

c) transmission spectra of sample S-3

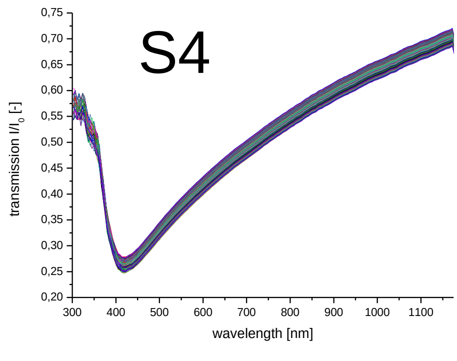

d) transmission spectra of sample S-4

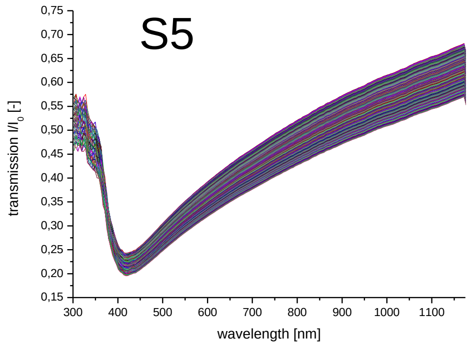	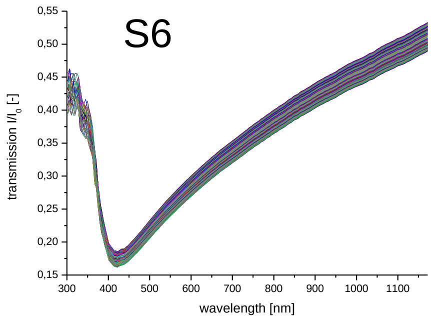
e) transmission spectra of sample S-5	f) transmission spectra of sample S-6

Figure 3.1.5.6: VIS-transmission spectra of PP/clay samples

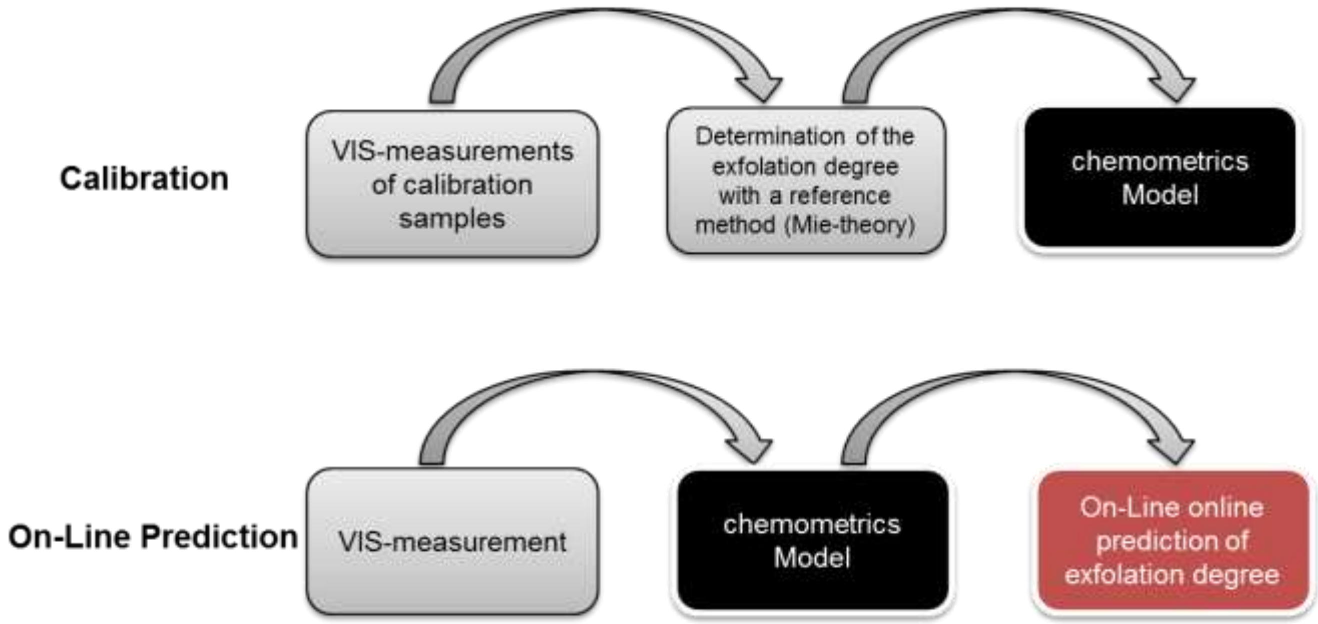

Figure 3.1.5.7: schematic view of generating prediction model for determination of exfoliation degree of the clays by VIS spectroscopy

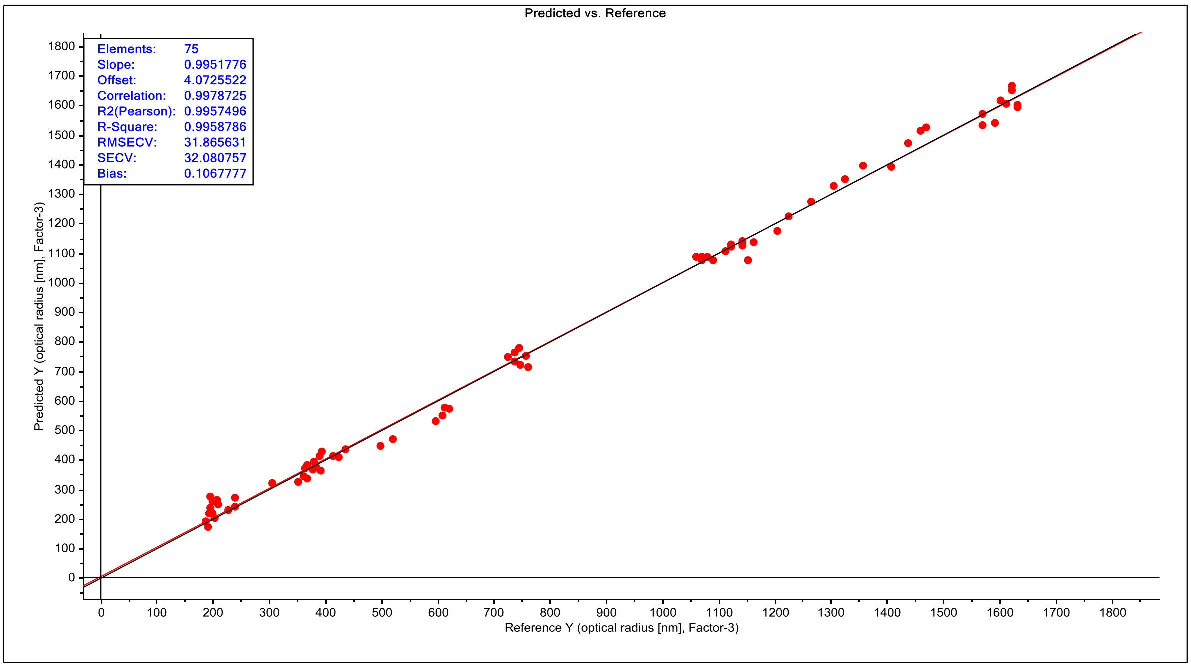

Figure 3.1.5.8: Prediction of exfoliation degree vs. reference exfoliation degree (determined by turbidimetric method).

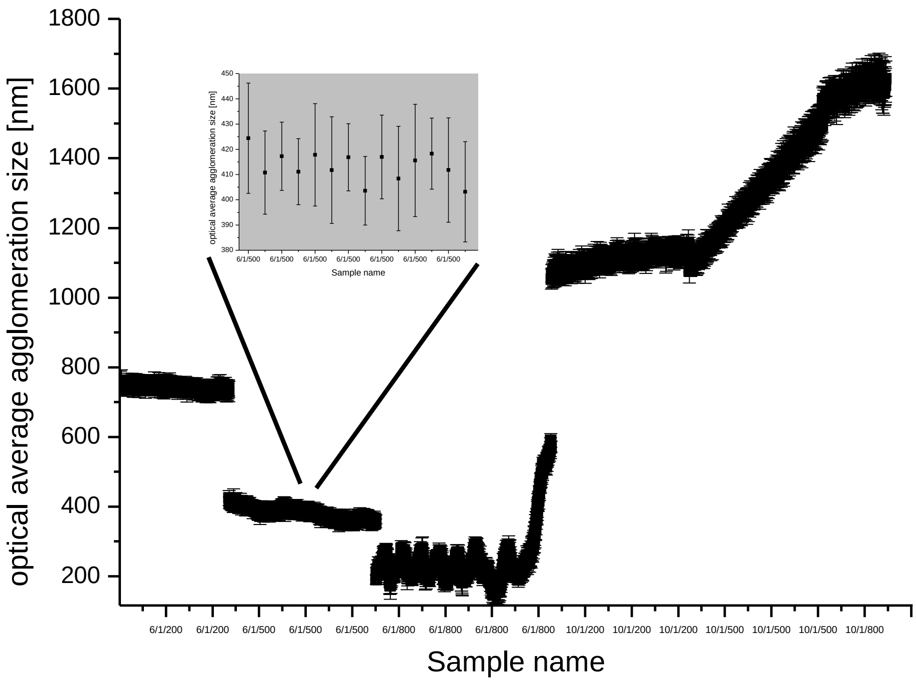

Figure 3.1.5.9: The prediction of the optical average agglomeration particle size (exfoliation degree of the clays) of 2469 spectra by PLS-model.

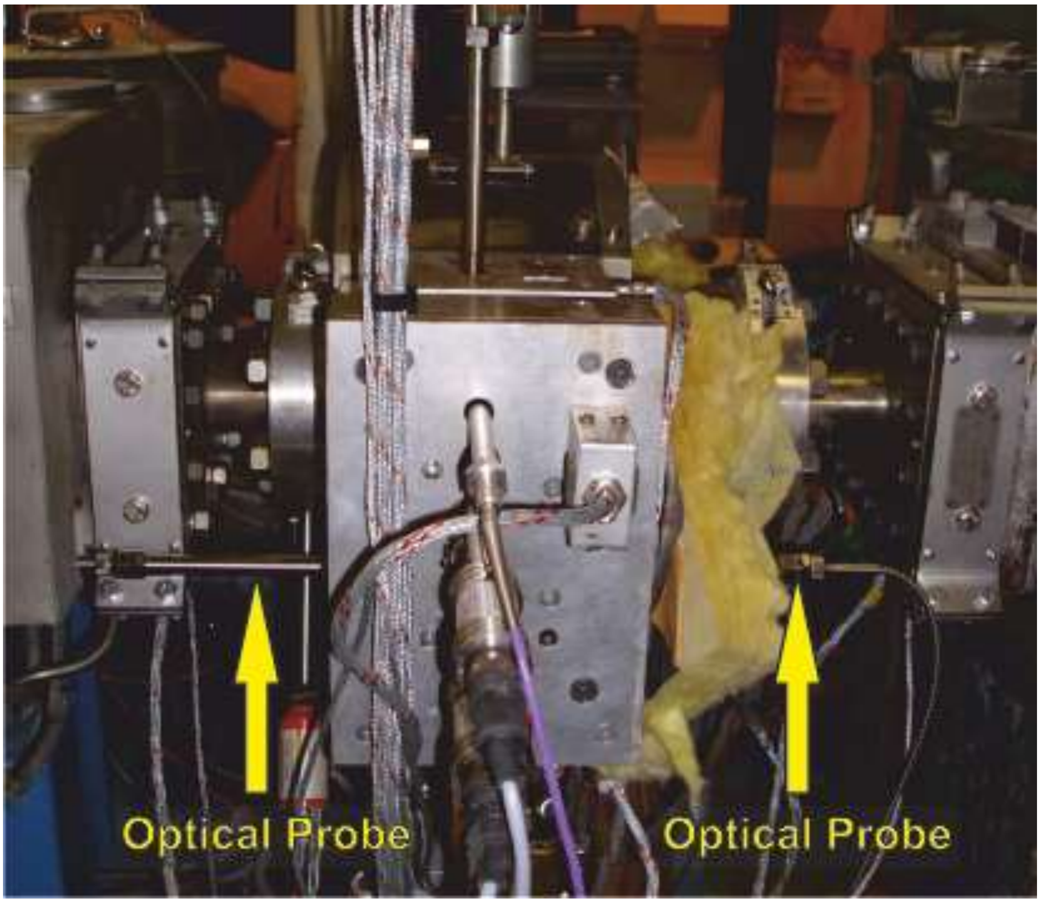

Figure 3.1.5.10: FOS optical transmission probes mounted at the OnBox-Unit.

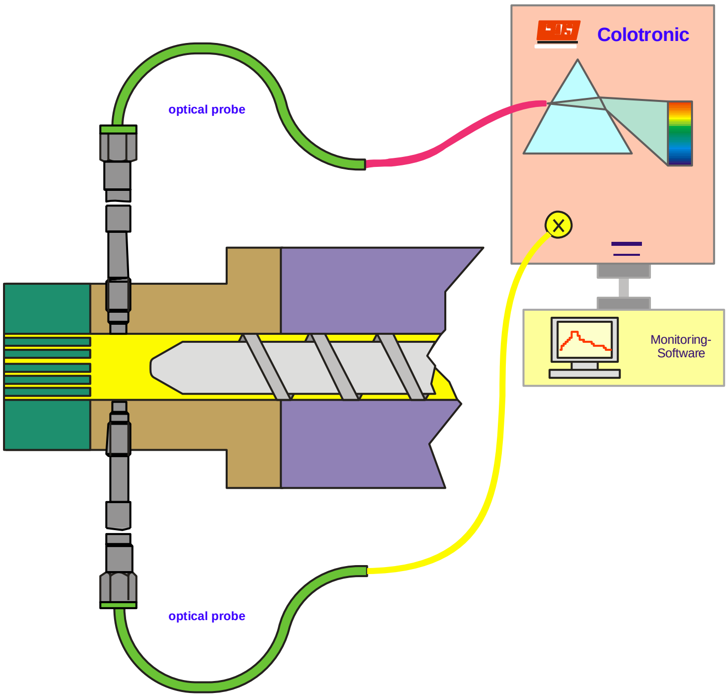

Figure 3.1.5.11: Measuring setup for transmission mode spectroscopy.

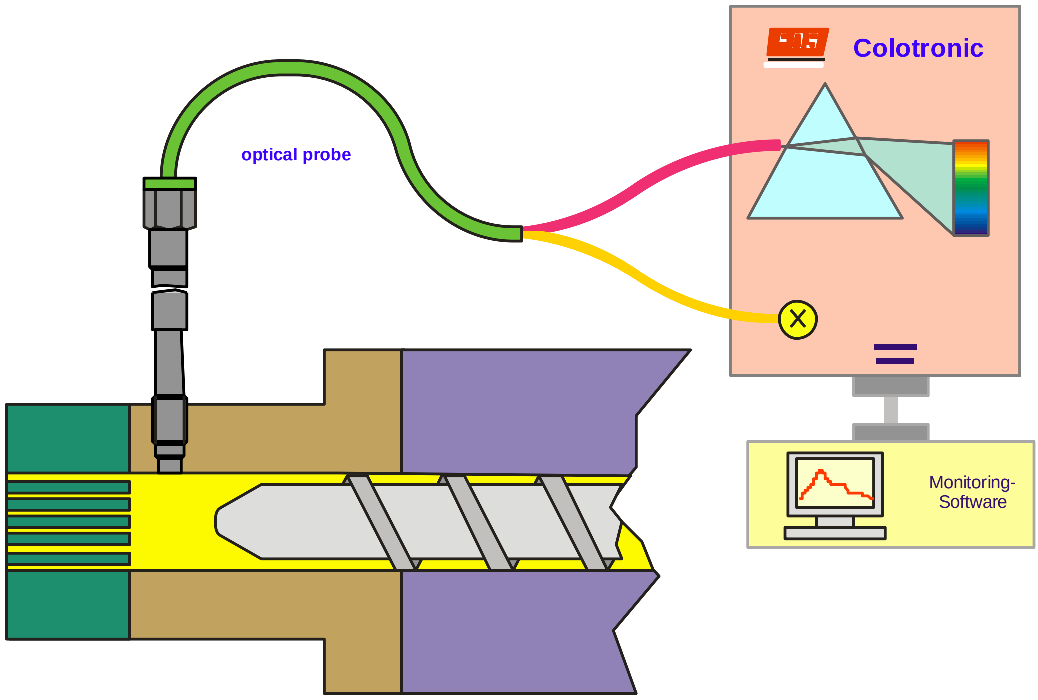

Figure 3.1.5.12: Measuring setup for reflection mode spectroscopy.

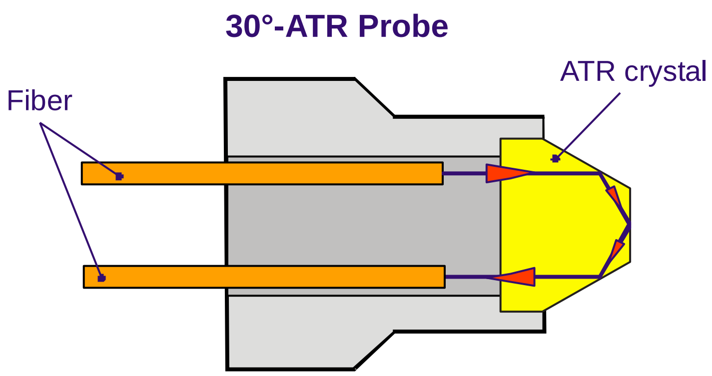

Figure 3.1.5.13: Principle of function of FOS ATR-NIR-FO-Probe with sapphire crystal tip.

Figure 3.1.5.14: Frontend of FOS ATR-NIR-FO-Probe with sapphire crystal tip.

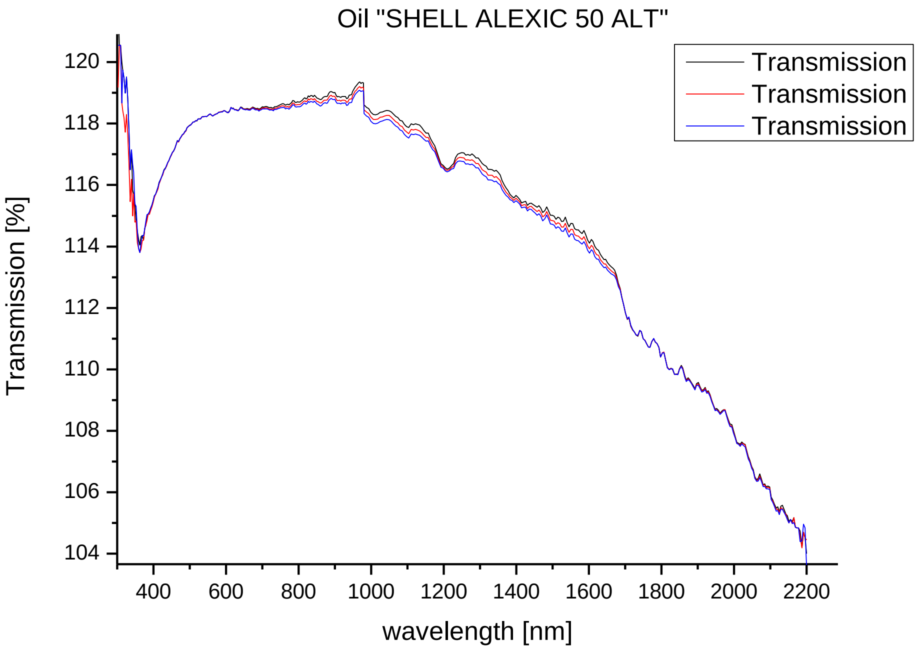

Figure 3.1.5.15 shows the spectral transmission of a 30°-ATR-probe when the probe tip is immersed in already used or aged motor oil. Motor oil is optically very similar to polymer melt.

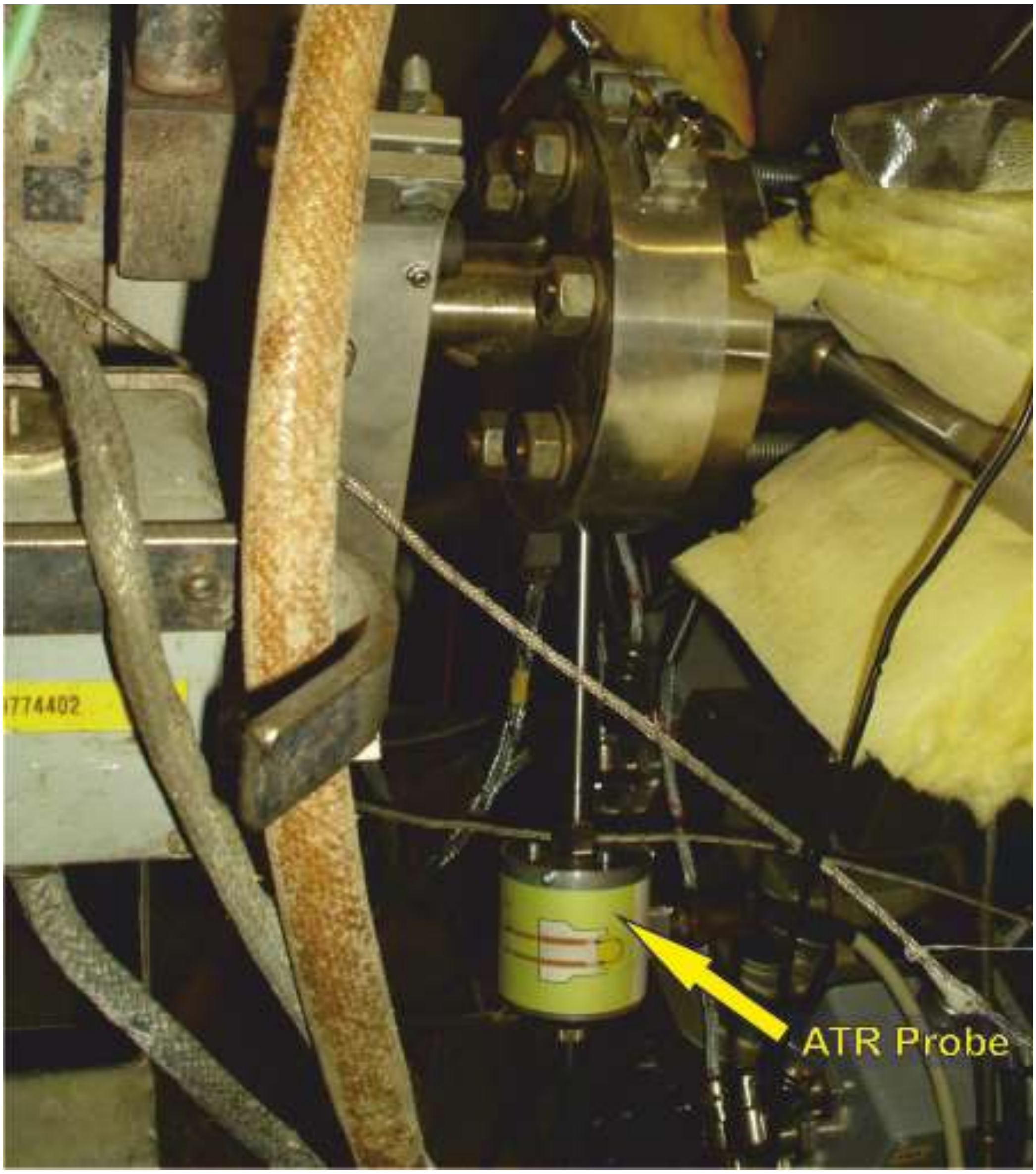

Figure 3.1.5.16: FOS ATR-NIR-FO-Probe mounted at an extruder for testing.

3.1.6 Ultrasonic sensing system (Ateknea)

Figure 3.1.6.1: Global view of the ultrasonic measurement system

Figure 3.1.6.2: Adapter and ultrasonic sensors

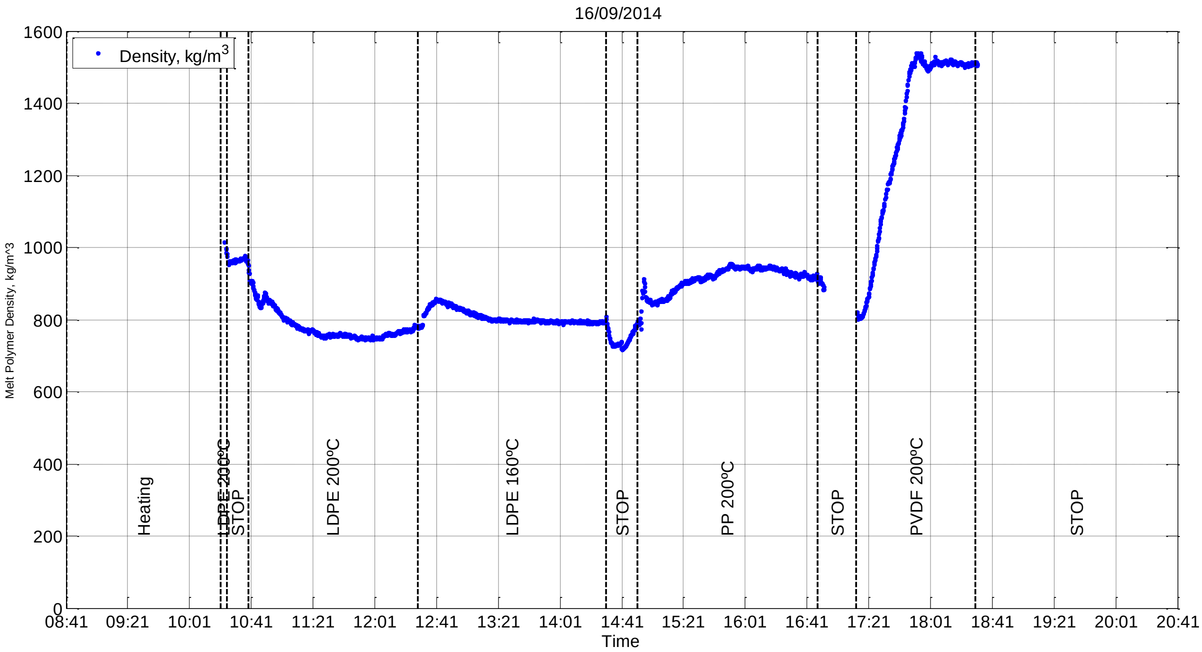

Figure 3.1.6.3: Density measurements of pure materials

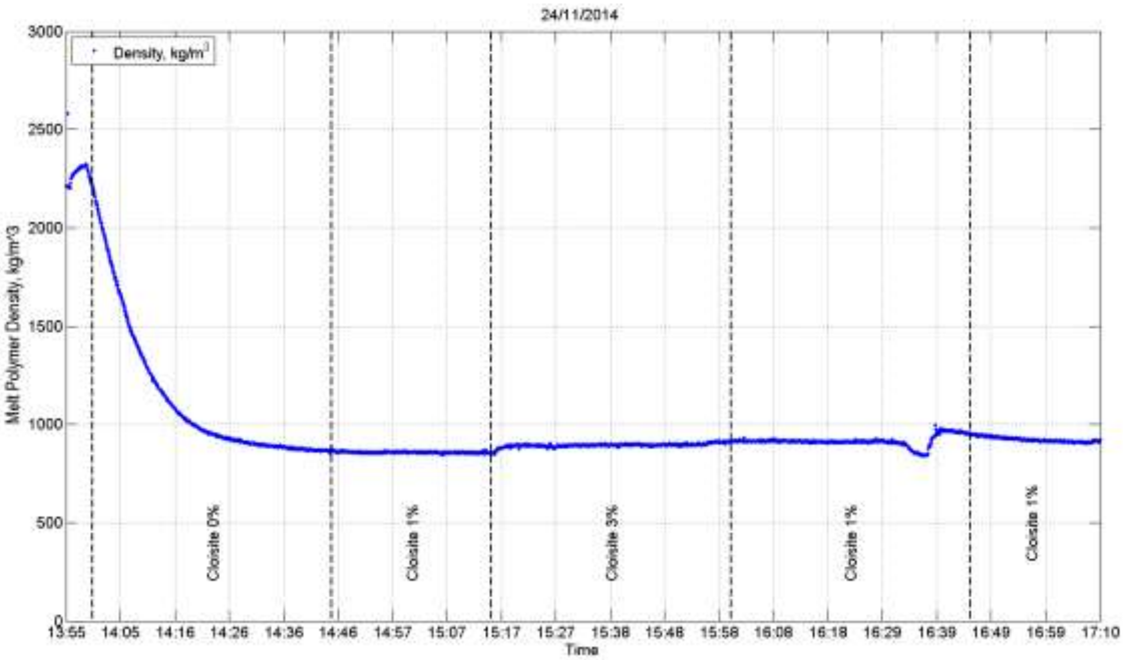

Figure 3.1.6.4: Density measurements of different blends of PP and cloisite

3.1.7 Microwave spectroscopy sensing system (ICT)

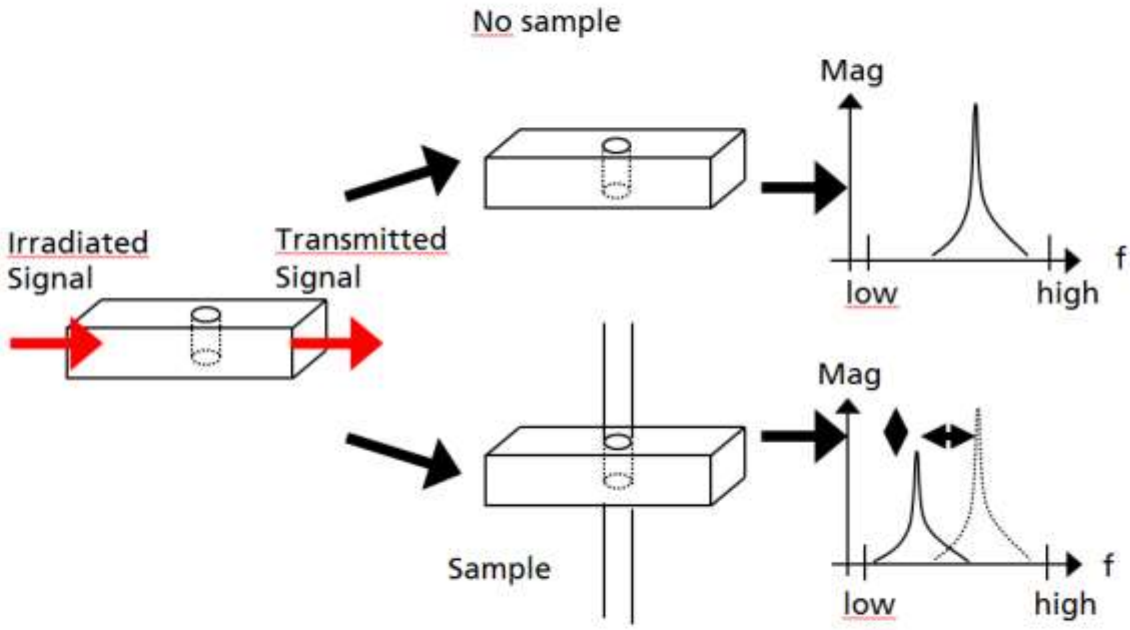

Figure 3.1.7.1: Schematic diagram of the cavity perturbation measurement principle

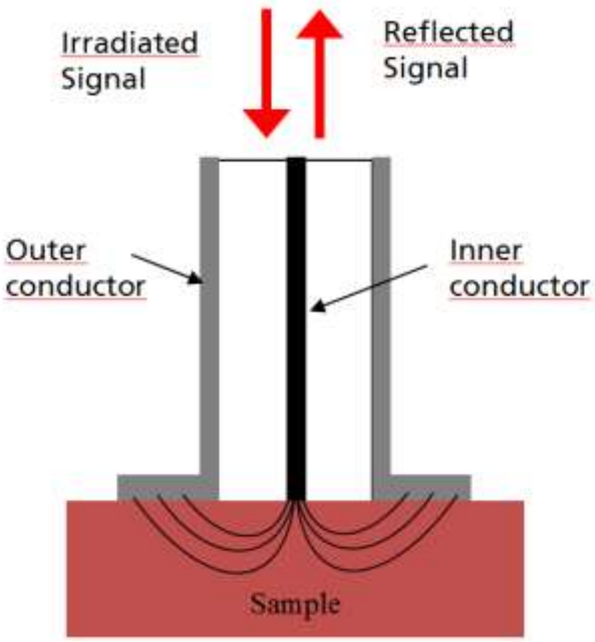

Figure 3.1.7.2: Schematic diagram of the Corbino measurement principle

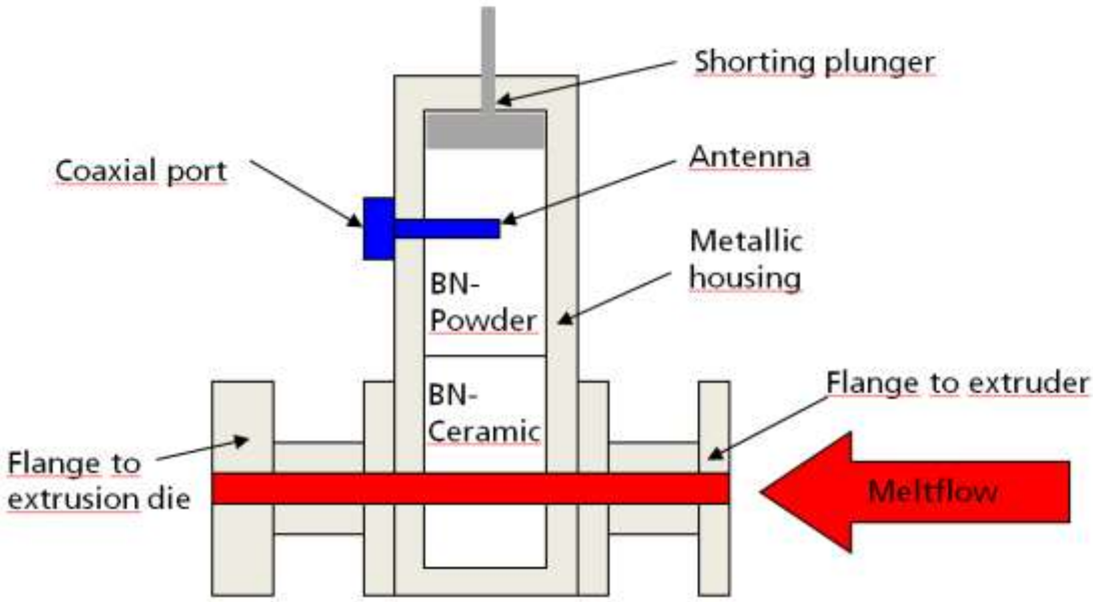

Figure 3.1.7.3: Schematic diagram of the resonant cavity sensor

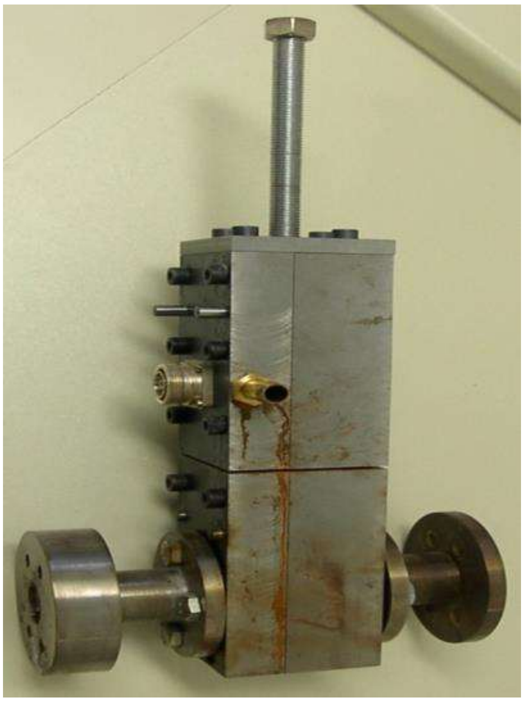

Figure 3.1.7.4: Resonant cavity sensor

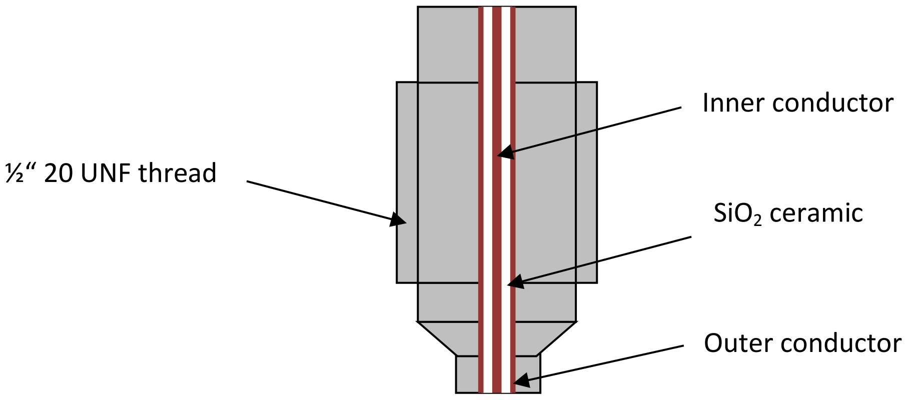

Figure 3.1.7.5: Schematic diagram of the Corbino sensor

Figure 3.1.7.6a: Corbino sensor tip

Figure 3.1.7.6b: Corbino sensor

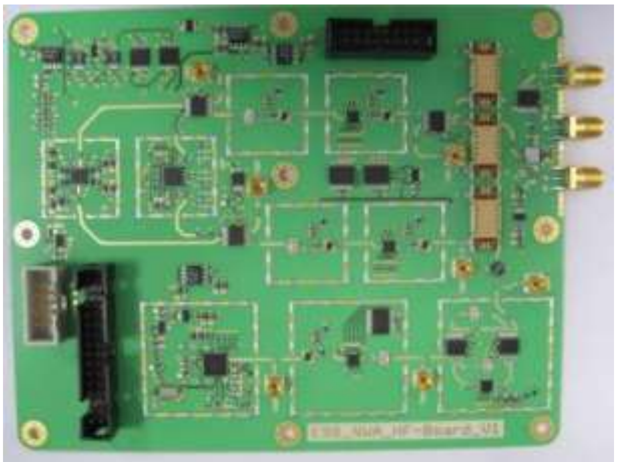

Figure 3.1.7.7a: Circuit board

Figure 3.1.7.7b: Measuring system with housing

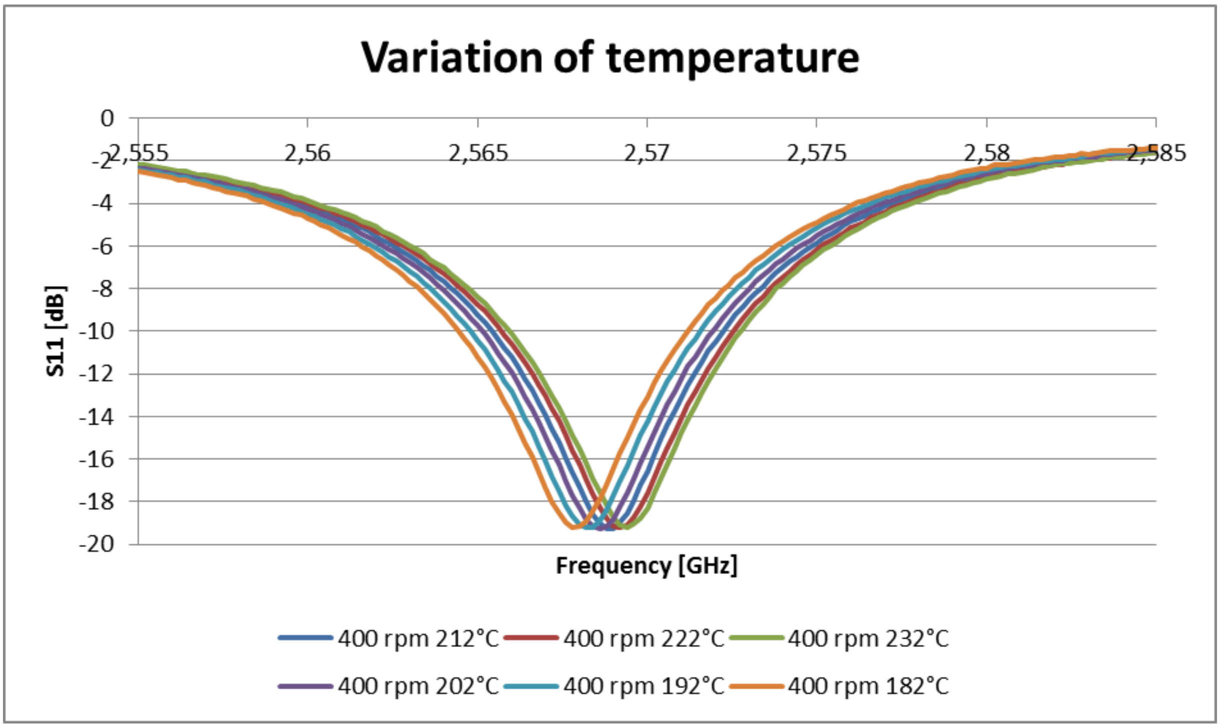

Figure 3.1.7.8: Variation of temperature on neat PP

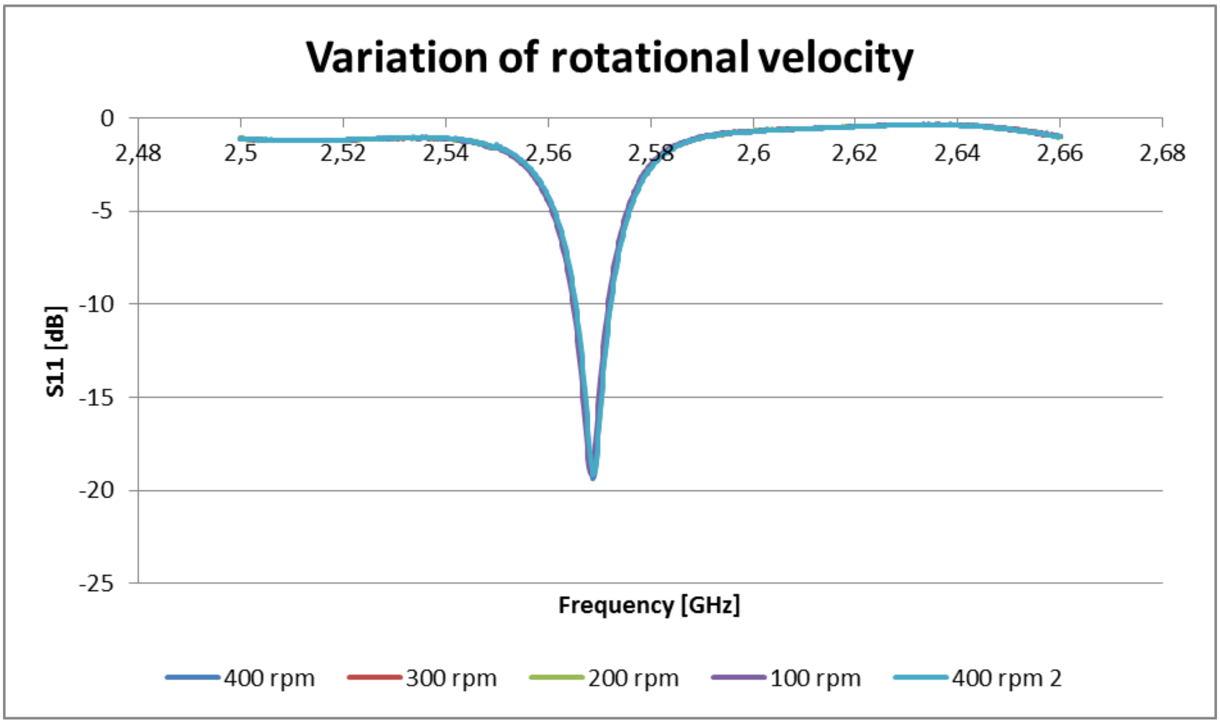

Figure **3.1.7.9: Variation of rotational velocity on neat PP**

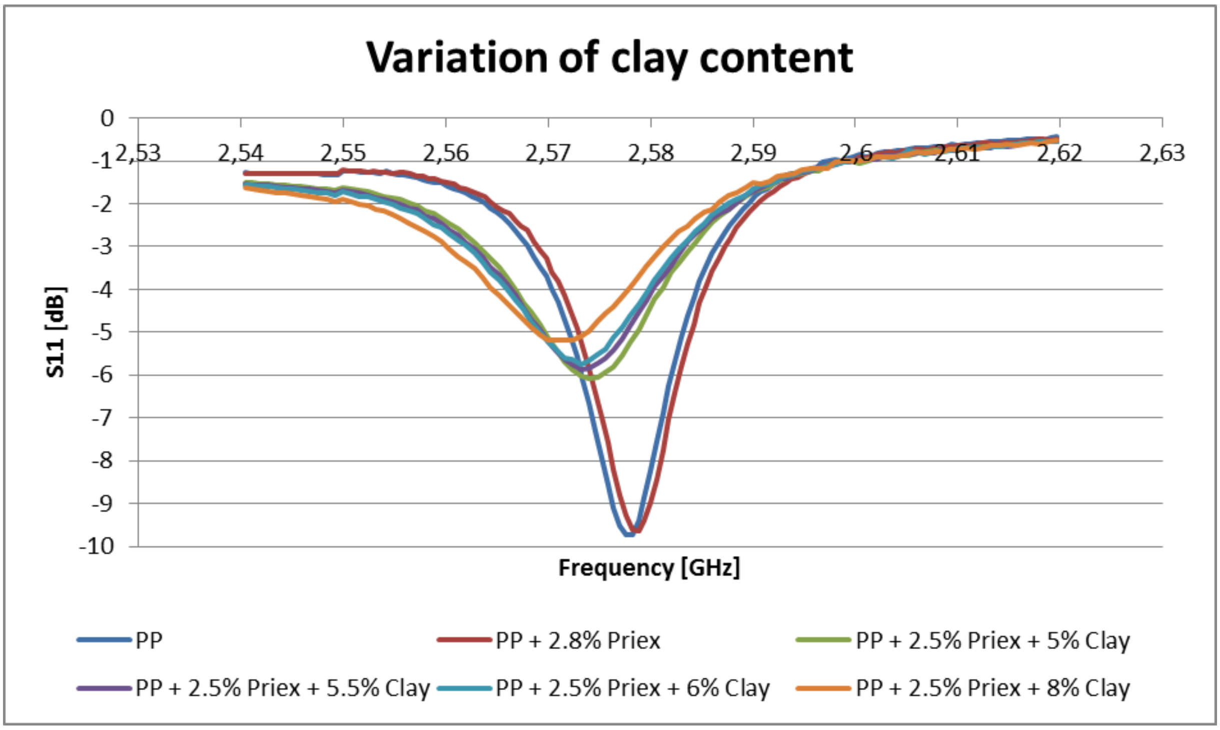

Figure 3.1.7.10 Variation of clay content in PP/Clay material system

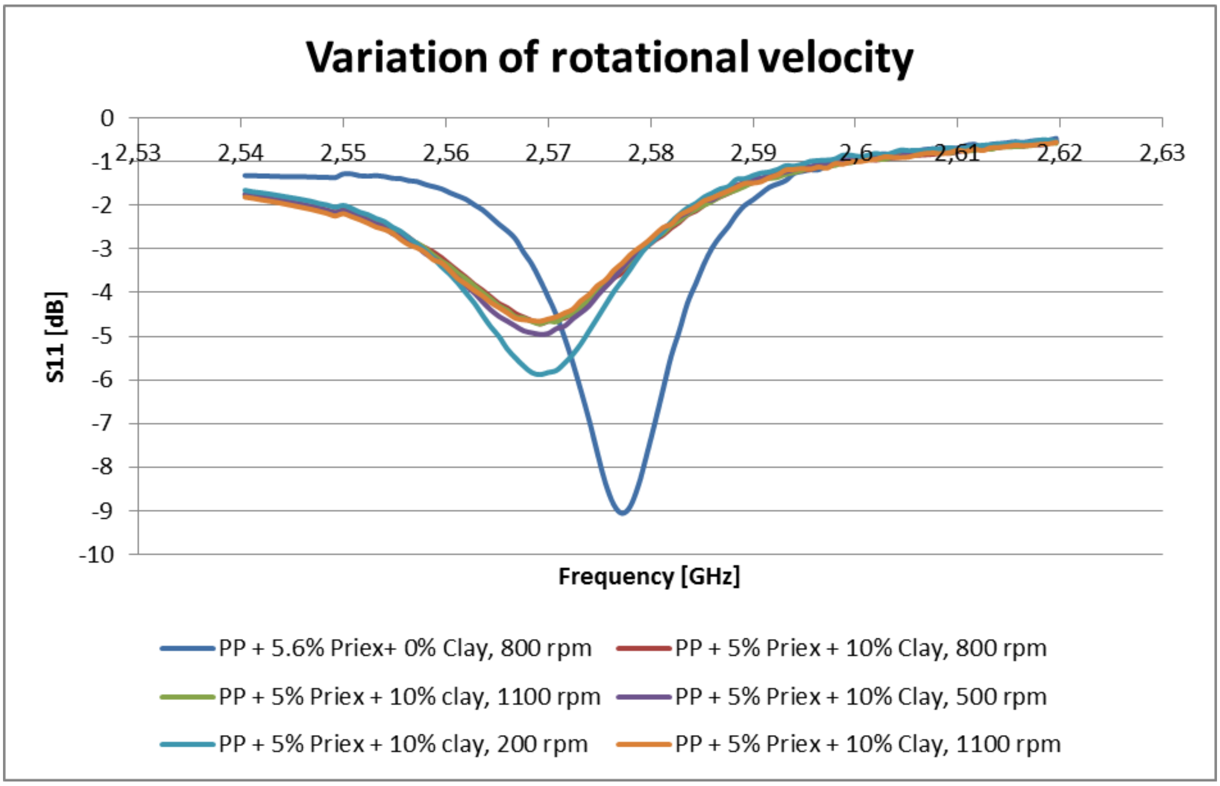

Figure 3.1.7.11: Variation of rotational velocity in PP/Clay material system

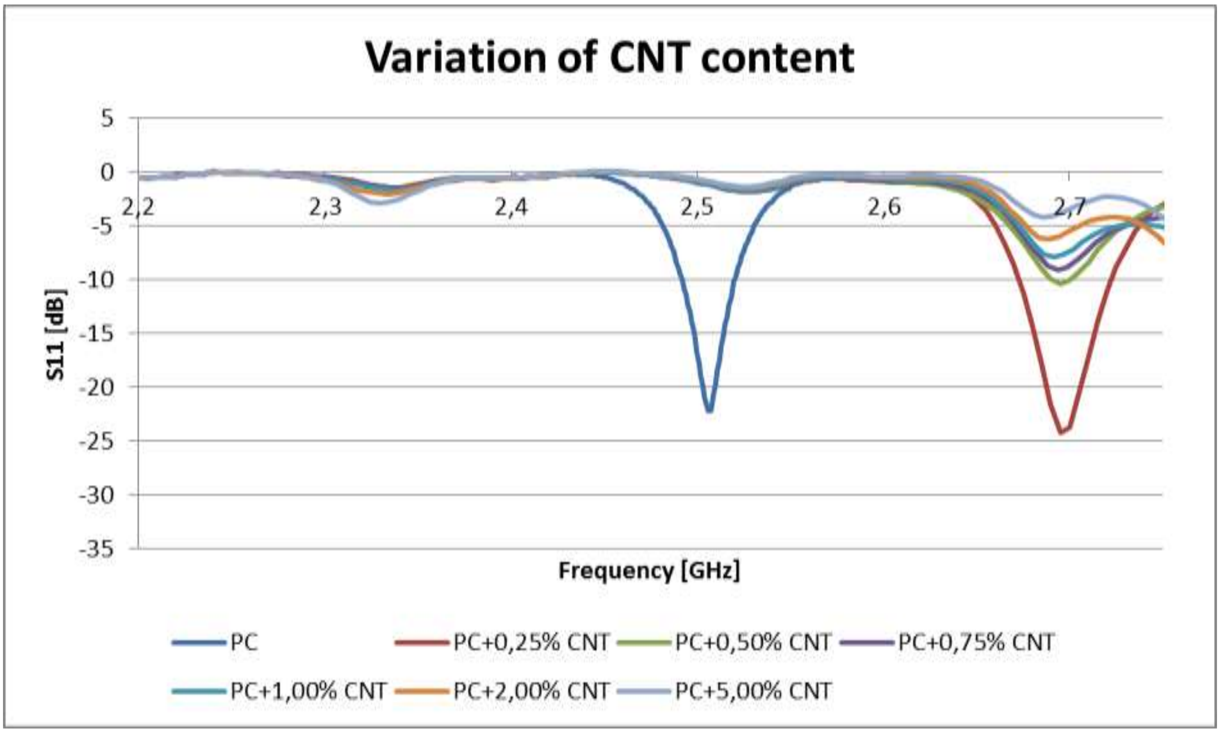

Figure 3.1.7.12: Variation of CNT content in PC/CNT material system

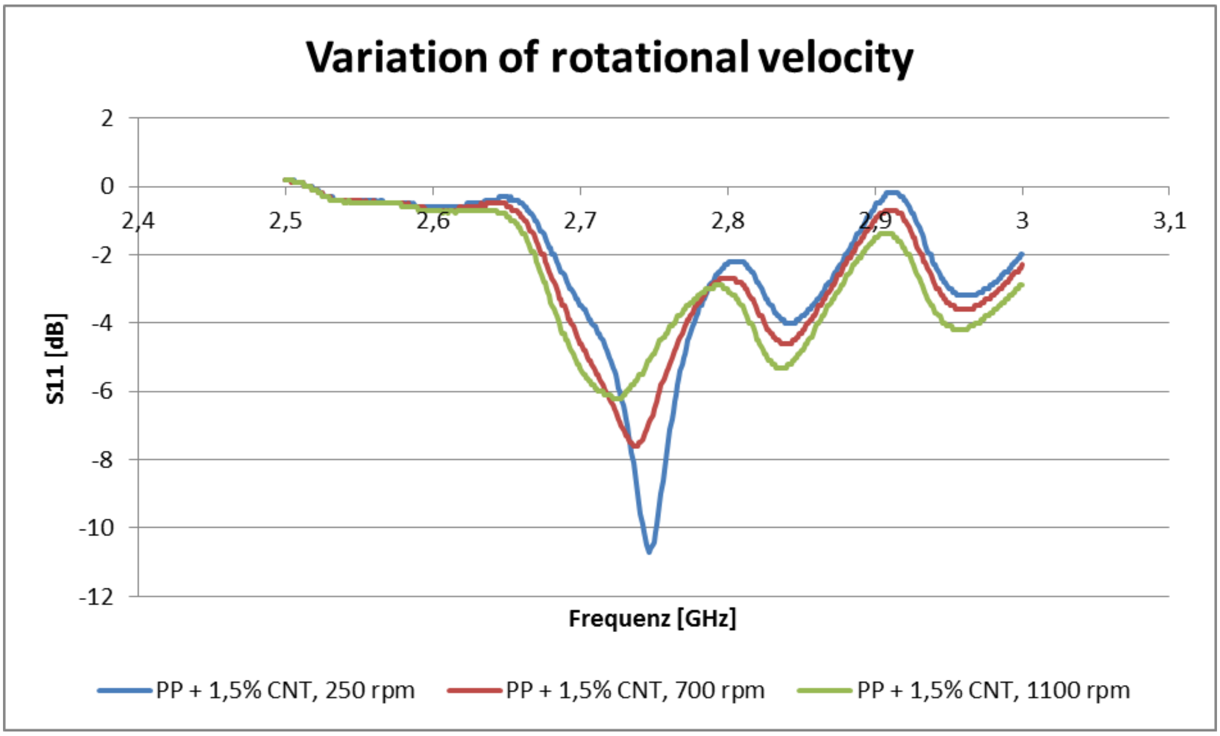

Figure 3.1.7.13: Variation of rotational velocity in PC/CNT material system

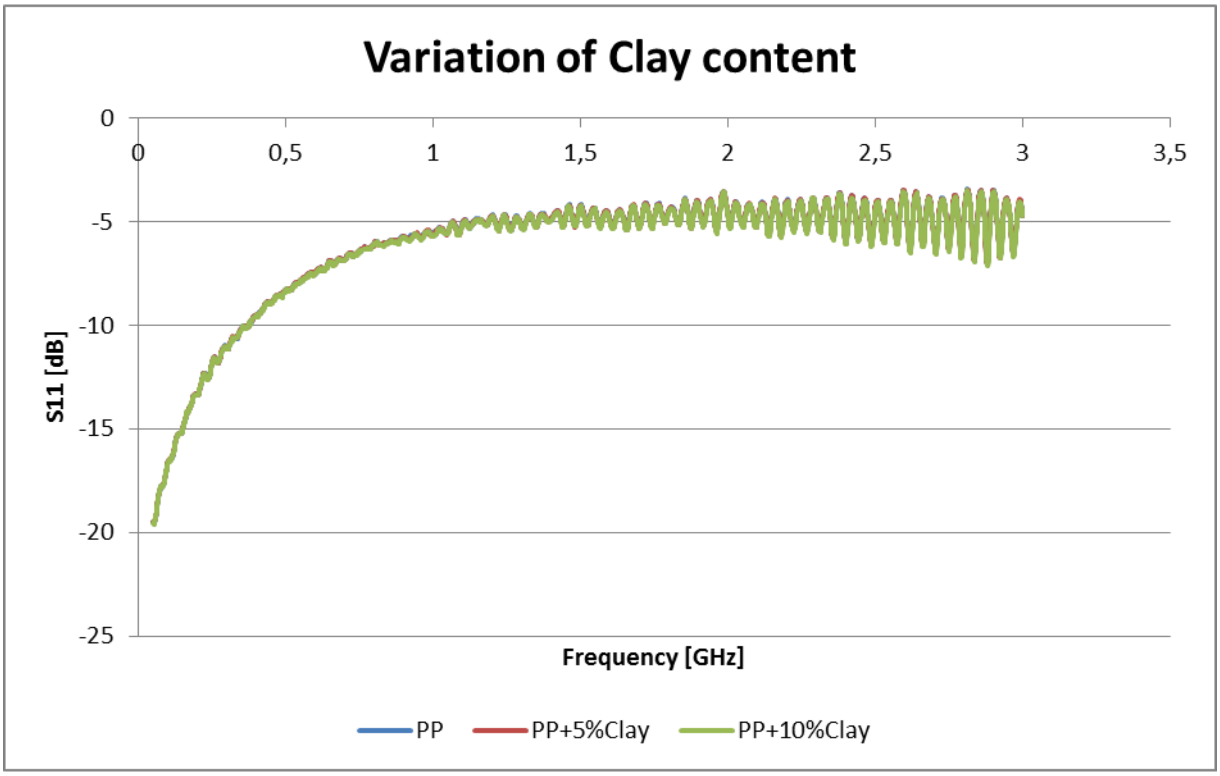

Figure 3.1.7.14: Variation of Clay content in PP/Clay material system

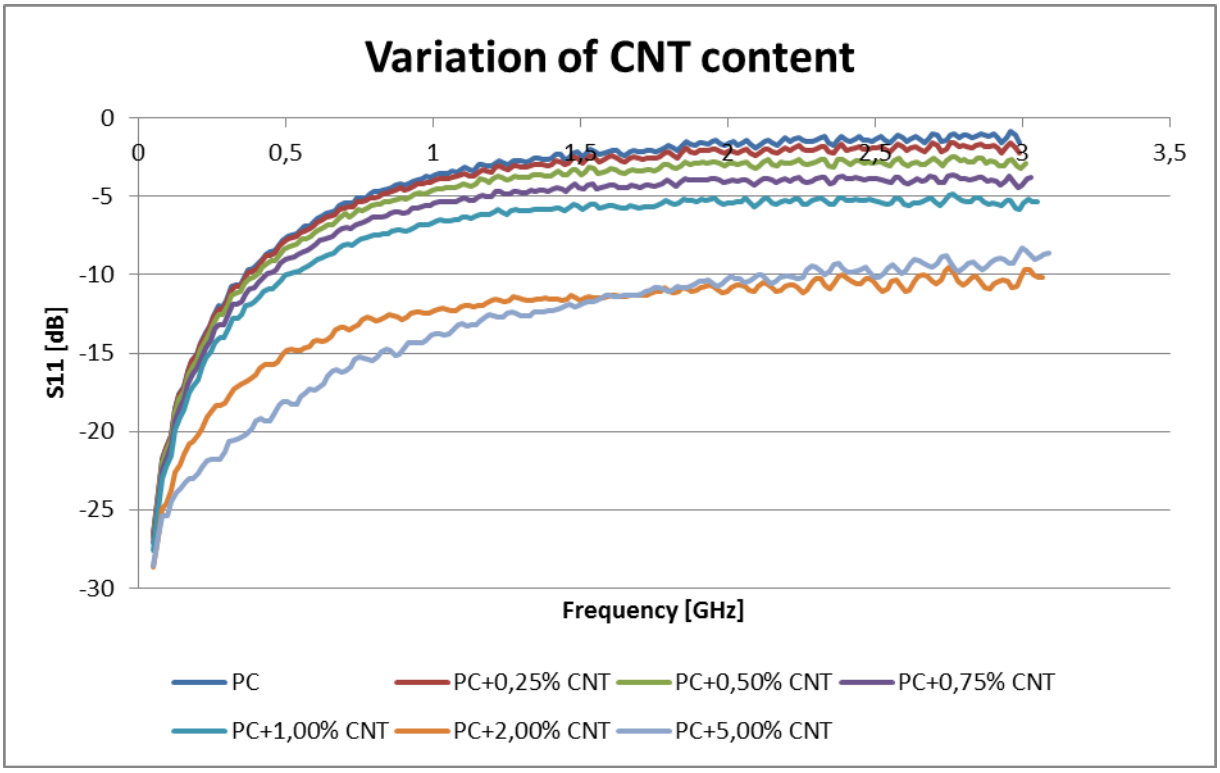

Figure 3.1.7.15: Variation of CNT content in PC/CNT material system

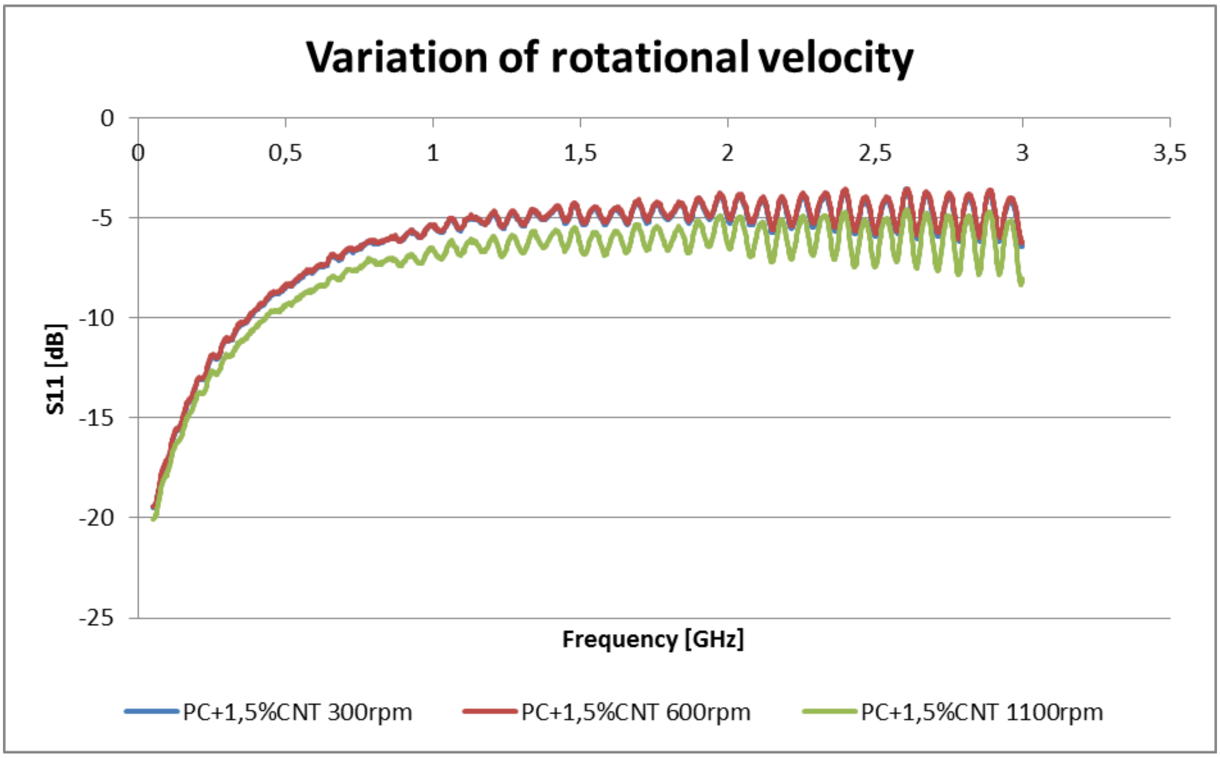

Figure 3.1.7.16: Variation of rotational velocity in PC/CNT material system

3.1.8 Development of the onBOX device (Gneuss)

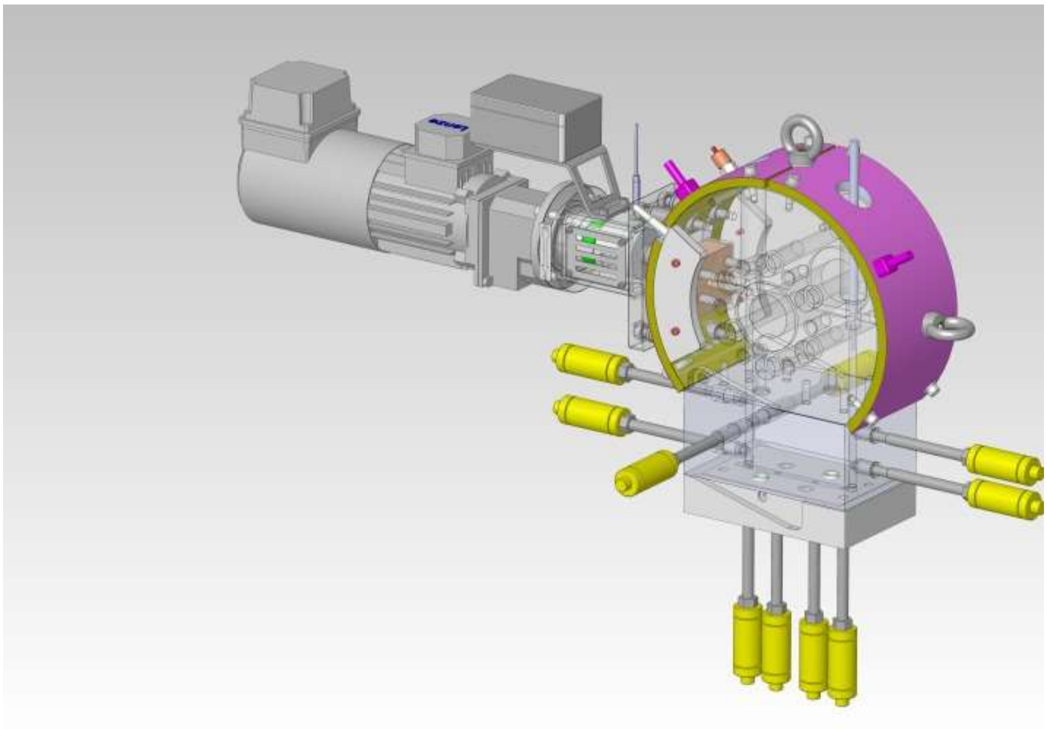

Figure 3.1.8.1: Rheology sensing unit with various sensors in sensor block for online side stream measurement.

3.2 WP2 New compounding process technology and automation

3.2.1 Main objectives

3.2.2 Nexxus compounding technology

Figure 3.2.2.1: Nexxus Melting and Mixing in cascade

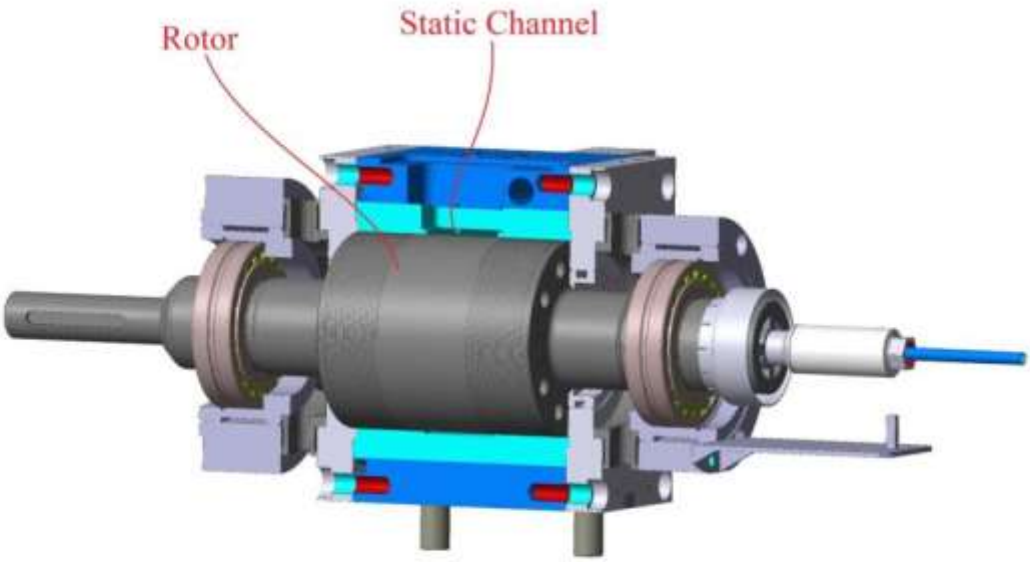

Figure 3.2.2.2 a: 3D view of the rotor

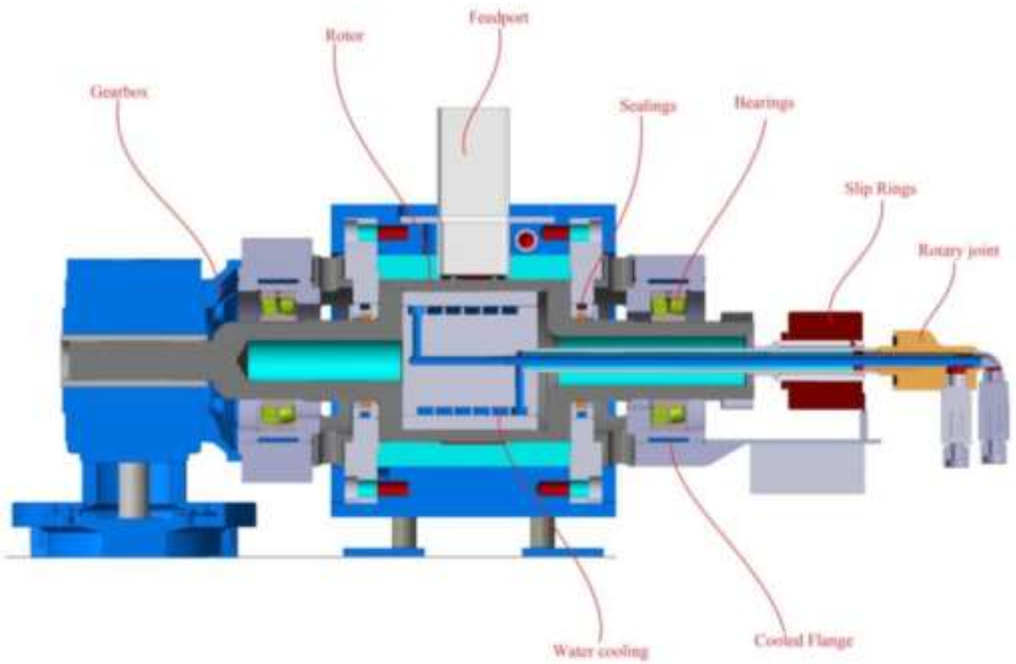

Figure 3.2.2.2b: Rotor section

(Polymer PP Homo Total 9760 MFI 24)

Throughput [kg/h]	RPM	Rotor speed [m/s]	Melting rate/rpm [Kg/hrpm]	Melting Model Tadmor [Kg/hrpm]	Total Kwh	Kw/hkg [SEC]	Temp- [°C]	End taper pressure [bar]
10	10,9	0,11	0,92	0,434	1,5	0,15	236/206	4
15	15,1	0,16	0,99	0,3755	1,65	0,11	235/202	4
25	29,0	0,30	0,86	0,327	2,85	0,114	235/201	4
40	78,7	0,82	0,51	0,36	6,1	0,153	233/202	4
50	108,9	1,14	0,46	0,355	8,4	0,168	235/220	5

Figure 3.2.2.3a: Melting rate vs speed compared with the familiar Tadmor's model

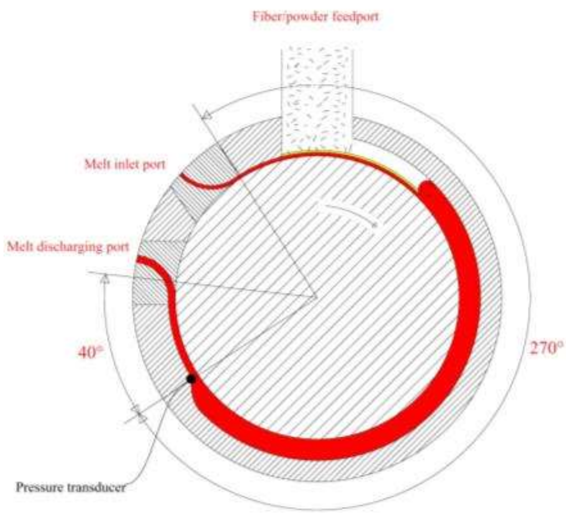	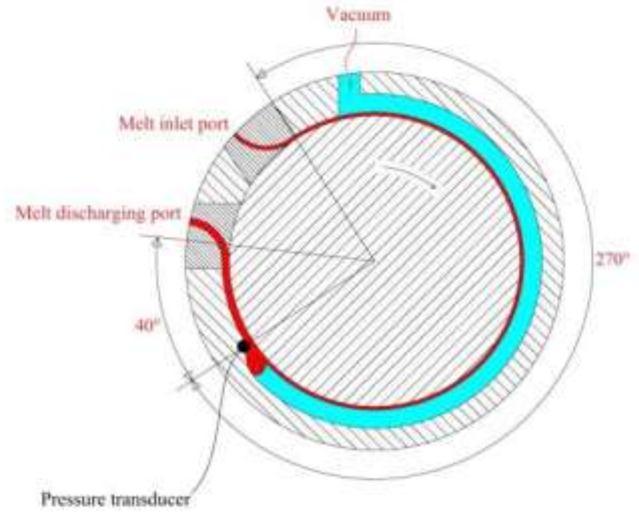
$Rt = \dfrac{Vol\Phi}{Q_{vol}}$ where: • Vol=chamber volume [m^3] • Φ=adimensional filling factor [0:1] • Qvol= volumetric flow rate [m^3/s]	$\lambda = \dfrac{H^2}{D'}$ where: • λ= characteristic diffusion time [s] • H= film thickness [m] • D'= coeff. Diffusion [m^2/s]
Figure 3.2.2.3b	**Figure 3.3.2.2.c**

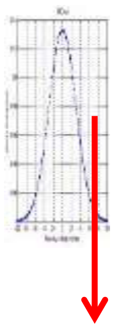

Not yet evaluated but estimated nearly around zero

Figure 3.2.2.3d

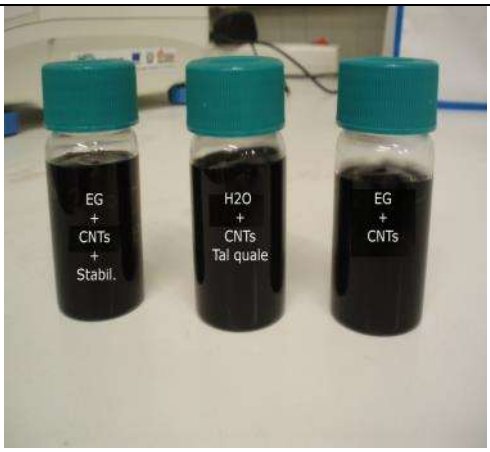

Figure 3.2.2.4 .VOC powder vs VOC liquids

Figure 3.2.2.5. Early tests with waterborne CNT dispersion processed in Nexxus ((July 2013)

Figure 3.2.2.6: Tests stage in Jan 2015

Figure 3.2.2.7: VMS arranged with Nexxus

Figure 3.2.2.8: VPS arranged directly with cTSE HP18 Leistritz


Figure 3.2.2.9: On line measurement of melt resistivity

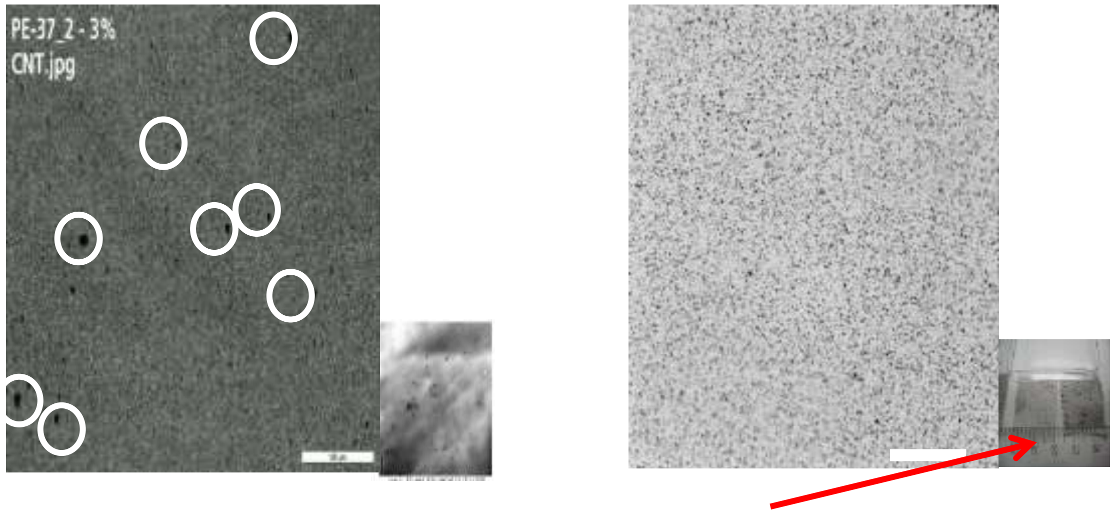

Figure 3.2.2.10: Optical evidence of superior CNT dispersion with Nexxus-VMS technology

3.2.1 Optimised conventional extrusion techniques

3.3 WP3 Material and process characterisation

3.3.1 Main objectives

3.3.2 Polycarbonate – CNT material system

3.3.3 Polypropylene – Clay material system

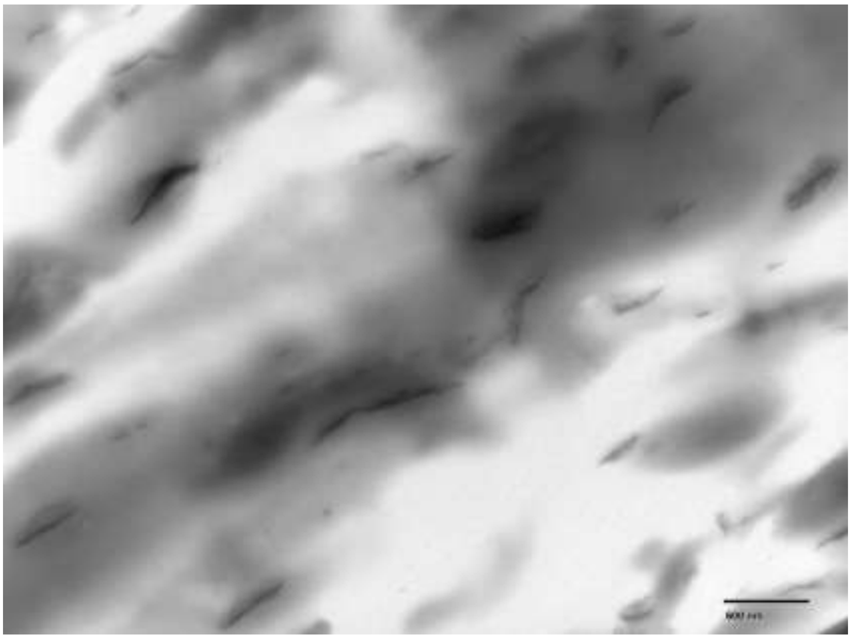

Figure 3.3.3.1: Pr1 6.200.190

3.4 WP4 Intelligent Module

3.4.1 Main objectives

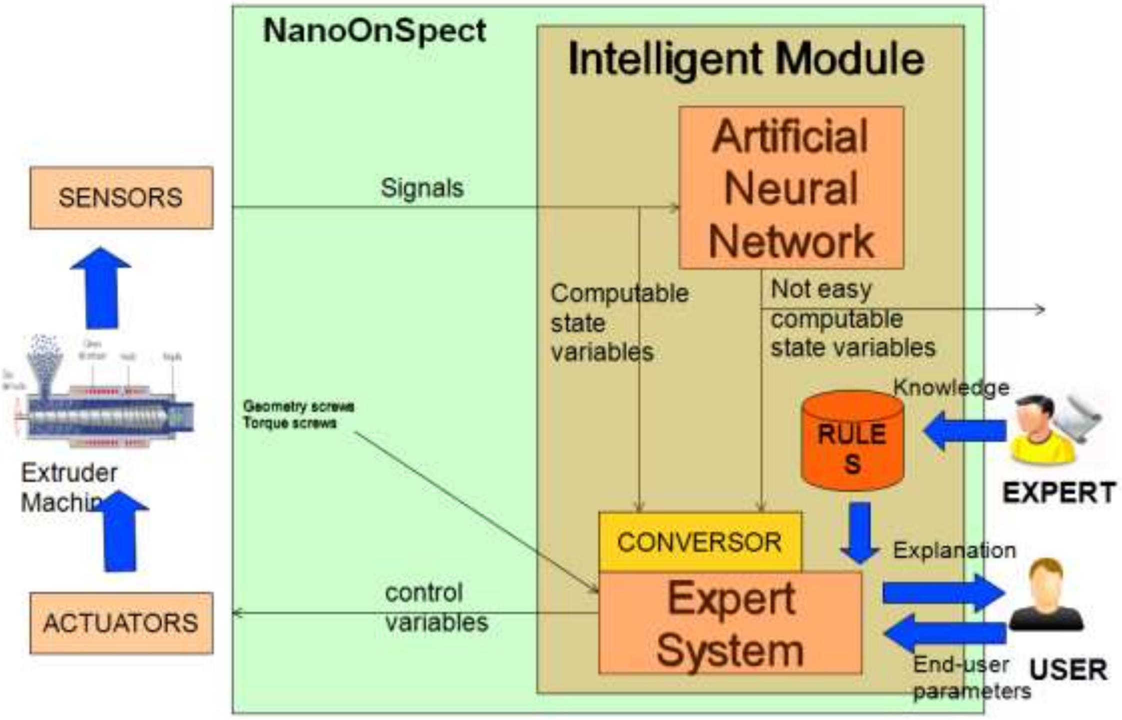

Figure 3.4.1.1. IM Software Architecture

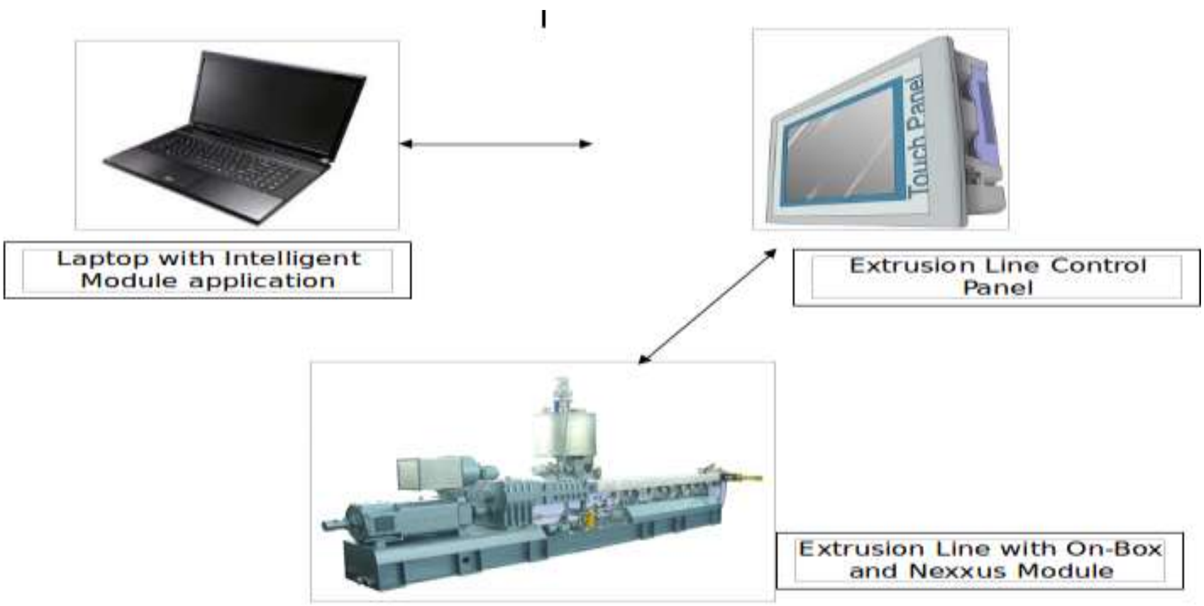

Figure 3.4.1.2. System Architecture

3.4.2 Artificial Neural Network

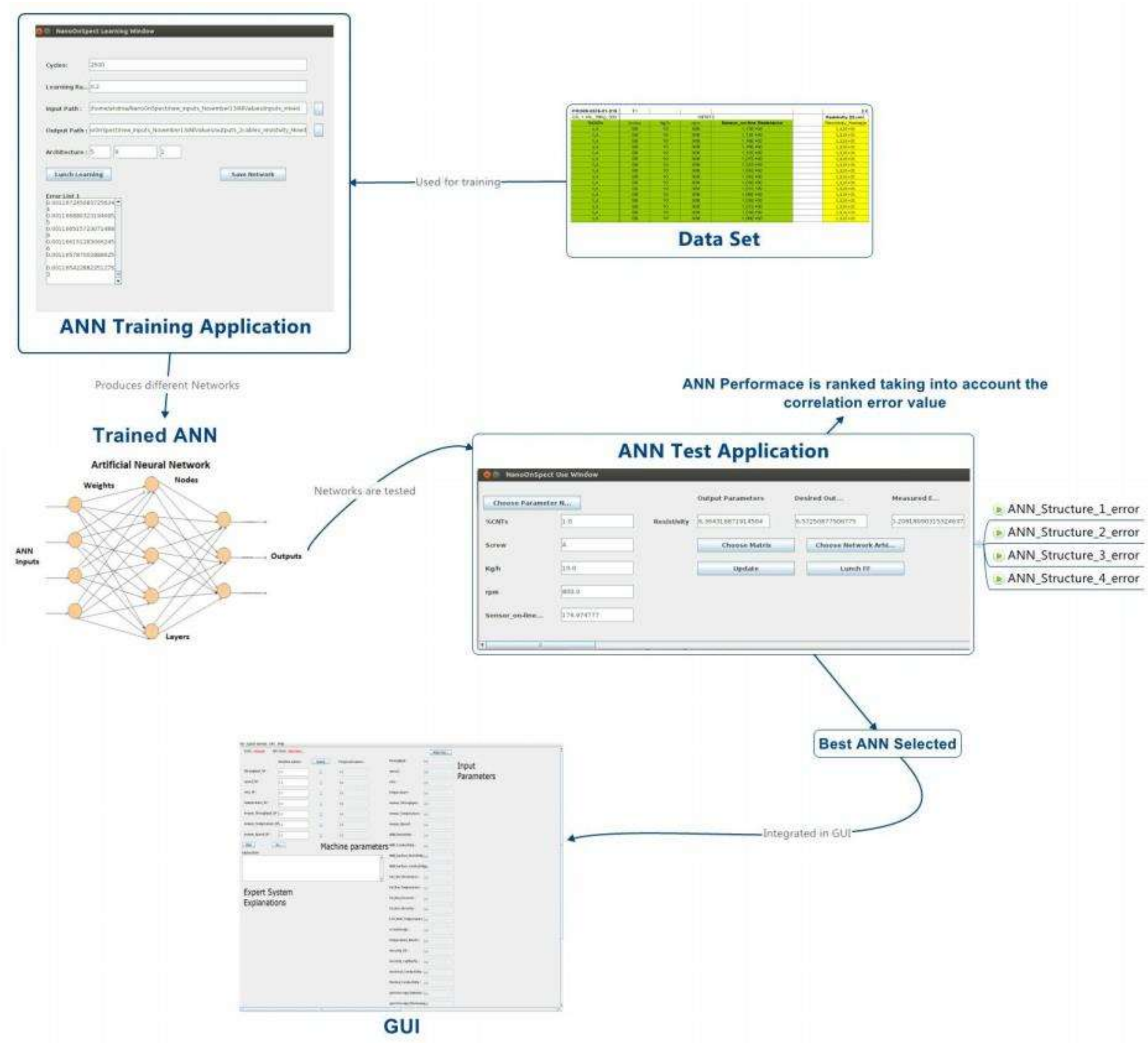

Figure 3.4.2 1. Artificial Network Training

Nº3_C-10-C1-300

Sample Nº	R(Multimetro)	Resistance[Ohm]	medidas pieza		l(dist. elect)	Resistivity[Ω*cm]	Average	Conductivity[S/cm]	Average	Ateknea Correlations		Absolute difference value ABS (Offline - On-line)	
	4 cables (ohm)	R(ohm)	b(ancho)(cm)	d(alto)(cm)		ρ=[b*d/l]*R	Resistivity	σ=1/ρ	Conductivity	Resistivity [Ω*cm] Average	Conductivity[S/cm] Average	Resistivity	Conductivity
1	51	5,100E+01	0,98	0,38	2,46	7,720E+00	7,569E+00	1,295E-01	1,323E-01	3,919E+00	2,297E-01	3,64994	0,09740
2	49	4,900E+01	0,98	0,38	2,46	7,418E+00		1,348E-01					
3	52	5,200E+01	0,98	0,38	2,46	7,872E+00		1,270E-01					
4	47	4,700E+01	0,98	0,38	2,46	7,115E+00		1,405E-01					
5	52	5,200E+01	0,98	0,38	2,46	7,872E+00		1,270E-01					
6	49	4,900E+01	0,98	0,38	2,46	7,418E+00		1,348E-01					

Nº4_C-10-C1-600

Sample Nº	R(Multimetro)	Resistance[Ohm]	medidas pieza		l(dist. elect)	Resistivity[Ω*cm]	Average	Conductivity[S/cm]	Average	Resistivity [Ω*cm] Average	Conductivity[S/cm] Average	Resistivity	Conductivity
	4 cables (ohm)	R(ohm)	b(ancho)(cm)	d(alto)(cm)		ρ=[b*d/l]*R	Resistivity	σ=1/ρ	Conductivity				
1	40	4,000E+01	0,98	0,38	2,46	6,055E+00	5,803E+00	1,651E-01	1,725E-01	3,619E+00	2,257E-01	2,18383	0,05323
2	39	3,900E+01	0,98	0,38	2,46	5,904E+00		1,694E-01					
3	37	3,700E+01	0,98	0,38	2,46	5,601E+00		1,785E-01					
4	37	3,700E+01	0,98	0,38	2,46	5,601E+00		1,785E-01					
5	39	3,900E+01	0,98	0,38	2,46	5,904E+00		1,694E-01					
6	38	3,800E+01	0,98	0,38	2,46	5,753E+00		1,738E-01					

Nº5_C-6-C1-600

Sample Nº	R(Multimetro)	Resistance[Ohm]	medidas pieza		l(dist. elect)	Resistivity[Ω*cm]	Average	Conductivity[S/cm]	Average	Resistivity [Ω*cm] Average	Conductivity[S/cm] Average	Resistivity	Conductivity
	4 cables (ohm)	R(ohm)	b(ancho)(cm)	d(alto)(cm)		ρ=[b*d/l]*R	Resistivity	σ=1/ρ	Conductivity				
1	50	5,000E+01	0,98	0,38	2,46	7,569E+00	7,695E+00	1,321E-01	1,300E-01	4,400E+00	2,007E-01	4,26806	0,07069
2	49	4,900E+01	0,98	0,38	2,46	7,418E+00		1,348E-01					
3	50	5,000E+01	0,98	0,38	2,46	7,569E+00		1,321E-01					
4	52	5,200E+01	0,98	0,38	2,46	7,872E+00		1,270E-01					
5	51	5,100E+01	0,98	0,38	2,46	7,720E+00		1,295E-01					
6	53	5,300E+01	0,98	0,38	2,46	8,023E+00		1,246E-01					

Nº6 C-6-C1-300

Sample Nº	R(Multimetro)	Resistance[Ohm]	medidas pieza		l(dist. elect)	Resistivity[Ω*cm]	Average	Conductivity[S/cm]	Average	Resistivity [Ω*cm] Average	Conductivity[S/cm] Average	Resistivity	Conductivity
	4 cables (ohm)	R(ohm)	b(ancho)(cm)	d(alto)(cm)		ρ=[b*d/l]*R	Resistivity	σ=1/ρ	Conductivity				
1	32	3,200E+01	0,98	0,38	2,46	4,844E+00	4,693E+00	2,064E-01	2,135E-01	6,284E+00	1,887E-01	1,59092	0,02482
2	29	2,900E+01	0,98	0,38	2,46	4,390E+00		2,278E-01					
3	31	3,100E+01	0,98	0,38	2,46	4,693E+00		2,131E-01					
4	30	3,000E+01	0,98	0,38	2,46	4,541E+00		2,202E-01					
5	31	3,100E+01	0,98	0,38	2,46	4,693E+00		2,131E-01					
6	33	3,300E+01	0,98	0,38	2,46	4,996E+00		2,002E-01					

Nº7_C-6-C1,5-600

Sample Nº	R(Multimetro)	Resistance[Ohm]	medidas pieza		l(dist. elect)	Resistivity[Ω*cm]	Average	Conductivity[S/cm]	Average	Resistivity [Ω*cm] Average	Conductivity[S/cm] Average	Resistivity	Conductivity
	4 cables (ohm)	R(ohm)	b(ancho)(cm)	d(alto)(cm)		ρ=[b*d/l]*R	Resistivity	σ=1/ρ	Conductivity				
1	36	3,600E+01	0,98	0,38	2,46	5,450E+00	5,702E+00	1,835E-01	1,755E-01	4,104E+00	2,270E-01	1,59839	0,05155
2	39	3,900E+01	0,98	0,38	2,46	5,904E+00		1,694E-01					
3	37	3,700E+01	0,98	0,38	2,46	5,601E+00		1,785E-01					
4	38	3,800E+01	0,98	0,38	2,46	5,753E+00		1,738E-01					
5	38	3,800E+01	0,98	0,38	2,46	5,753E+00		1,738E-01					
6	38	3,800E+01	0,98	0,38	2,46	5,753E+00		1,738E-01					

Nº8_C-6-C1,5-300

Sample Nº	R(Multimetro)	Resistance[Ohm]	medidas pieza		l(dist. elect)	Resistivity[Ω*cm]	Average	Conductivity[S/cm]	Average	Resistivity [Ω*cm] Average	Conductivity[S/cm] Average	Resistivity	Conductivity
	4 cables (ohm)	R(ohm)	b(ancho)(cm)	d(alto)(cm)		ρ=[b*d/l]*R	Resistivity	σ=1/ρ	Conductivity				
1	40	4,000E+01	0,98	0,38	2,46	6,055E+00	6,005E+00	1,651E-01	1,667E-01	3,698E+00	2,358E-01	2,30673	0,06906
2	39	3,900E+01	0,98	0,38	2,46	5,904E+00		1,694E-01					
3	40	4,000E+01	0,98	0,38	2,46	6,055E+00		1,651E-01					
4	39	3,900E+01	0,98	0,38	2,46	5,904E+00		1,694E-01					
5	42	4,200E+01	0,98	0,38	2,46	6,358E+00		1,573E-01					
6	38	3,800E+01	0,98	0,38	2,46	5,753E+00		1,738E-01					

Nº9_C-10-C1,5-300

Sample Nº	R(Multimetro)	Resistance[Ohm]	medidas pieza		l(dist. elect)	Resistivity[Ω*cm]	Average	Conductivity[S/cm]	Average	Resistivity [Ω*cm] Average	Conductivity[S/cm] Average	Resistivity	Conductivity
	4 cables (ohm)	R(ohm)	b(ancho)(cm)	d(alto)(cm)		ρ=[b*d/l]*R	Resistivity	σ=1/ρ	Conductivity				
1	39	3,900E+01	0,98	0,38	2,46	5,904E+00	5,626E+00	1,694E-01	1,784E-01	3,698E+00	2,369E-01	1,92773	0,05849
2	41	4,100E+01	0,98	0,38	2,46	6,207E+00		1,611E-01					
3	36	3,600E+01	0,98	0,38	2,46	5,450E+00		1,835E-01					
4	37	3,700E+01	0,98	0,38	2,46	5,601E+00		1,785E-01					
5	34	3,400E+01	0,98	0,38	2,46	5,147E+00		1,943E-01					
6	36	3,600E+01	0,98	0,38	2,46	5,450E+00		1,835E-01					

Figure 3.4.2.2 Artificial Neural Network Case Study Correlations

3.4.3 Expert System

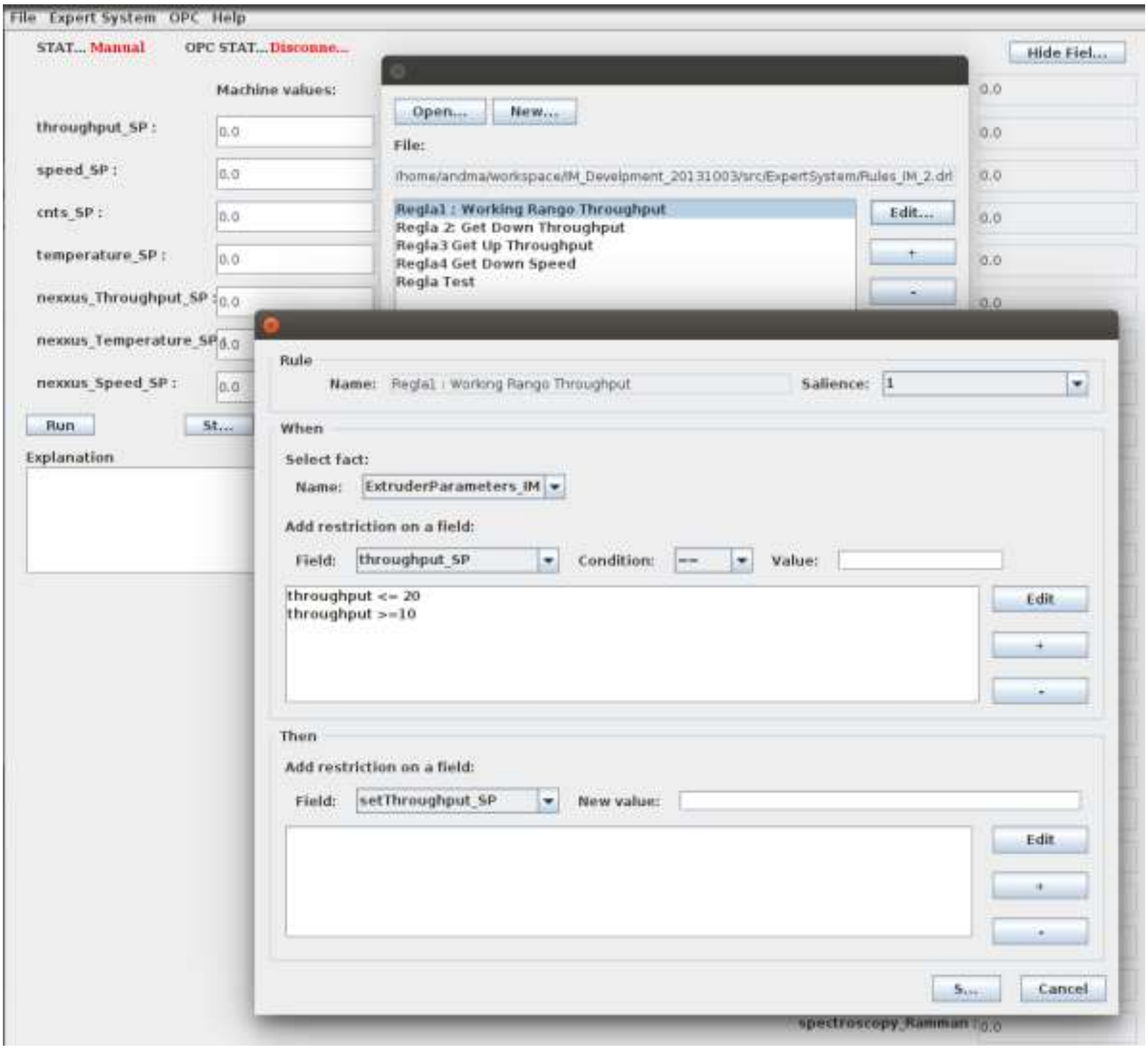

Figure 3.4.3.1: Expert System Rules editing interface

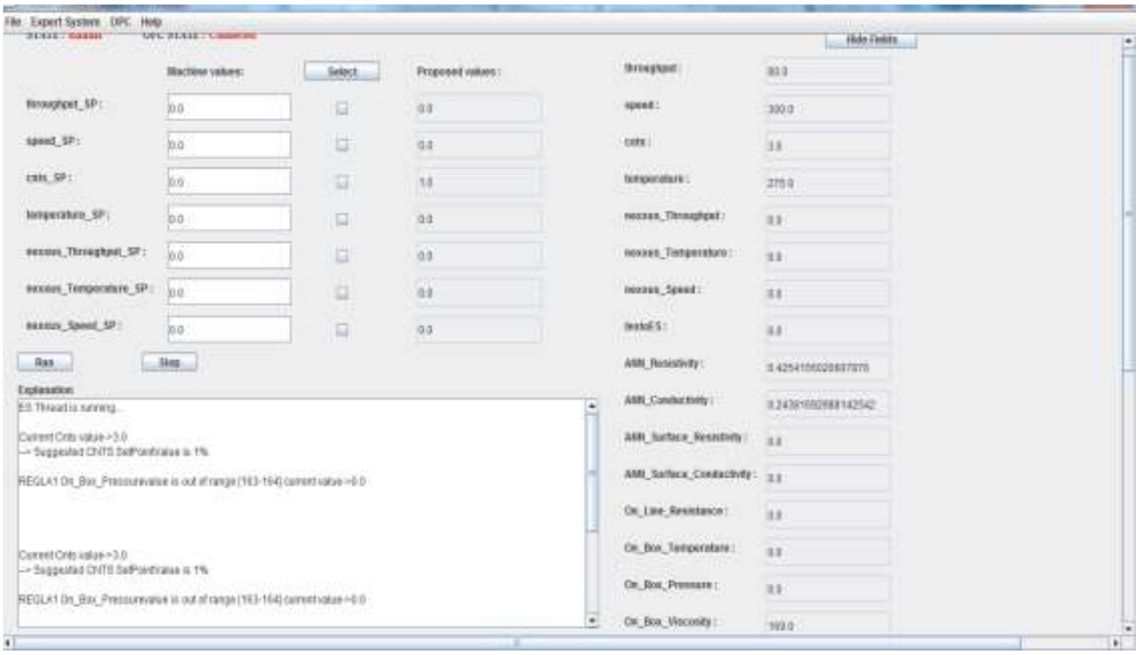

Figure 3.4.3.2. Viscosity value = 169, Cnts = 3.0, Expert System suggest Cnts=1

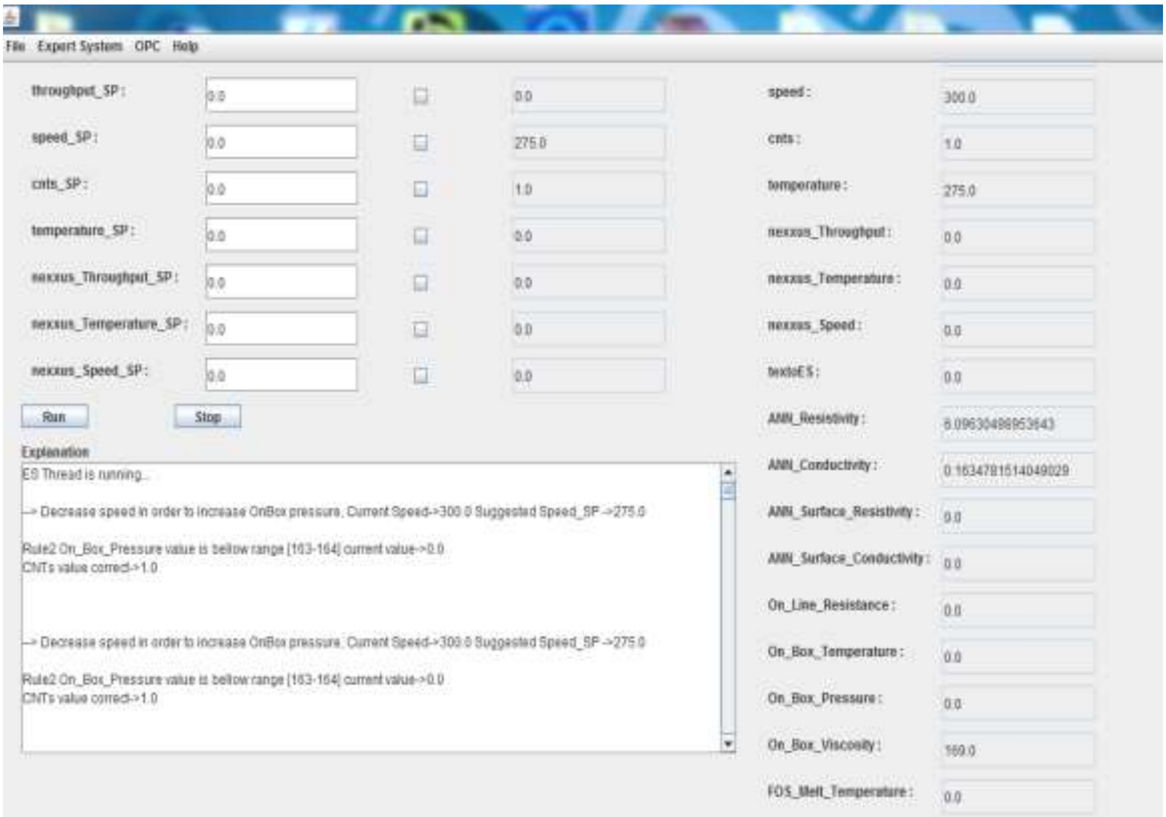

Figure 3.4.3.3: Viscosity value = 169, Cnts = 1.0, Expert System suggest Speed_SP =275

3.5 WP5 Application development and industrial case studies

3.5.1 Main objectives

3.5.2 Case Study Polycarbonate - CNT

Figure 3.5.2.1: Extrusion line Berstorff ZE 25 at Colorex Master Batch B.V.

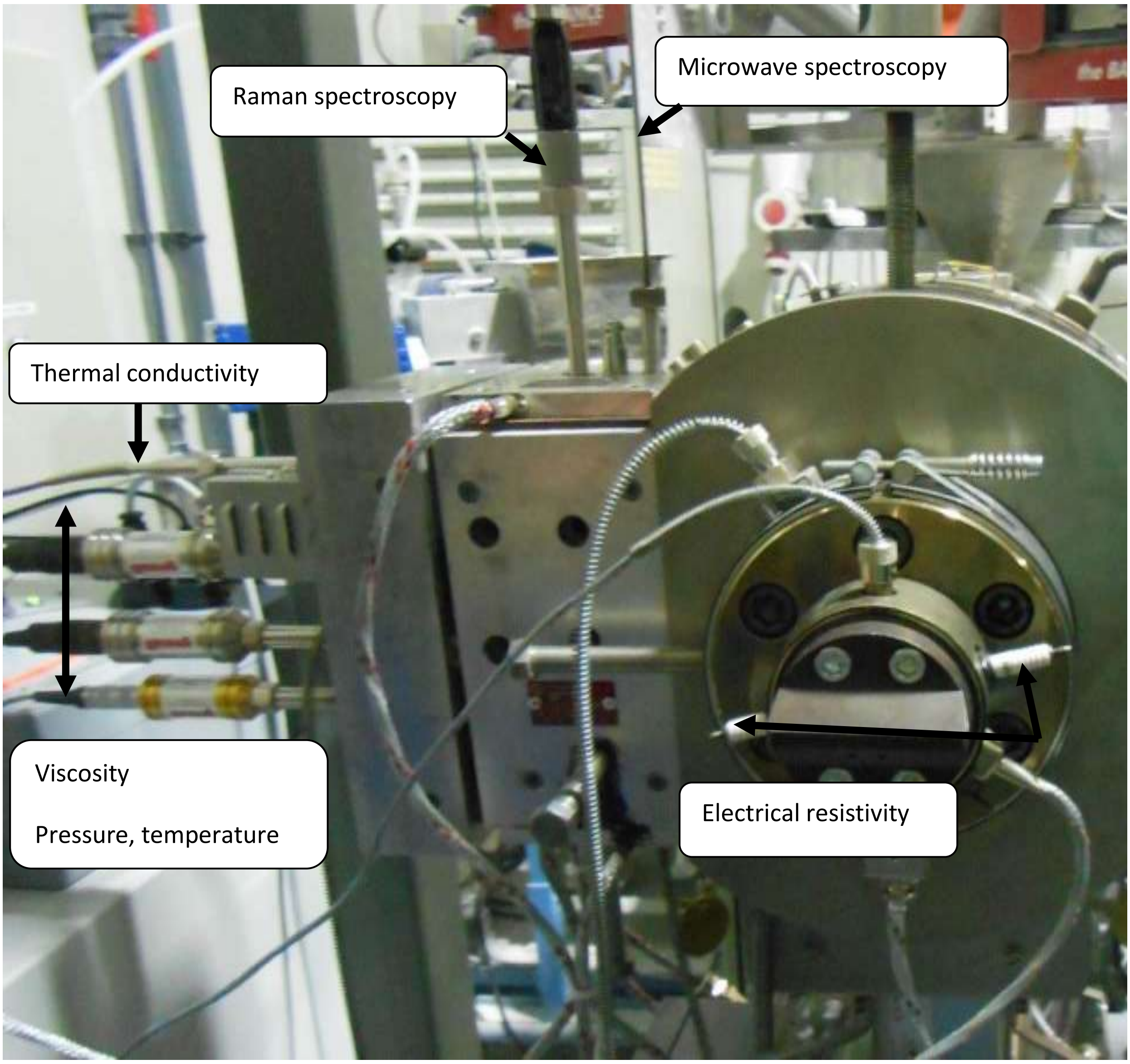

Figure 3.5.2.2: ^{on}BOX with installed sensors

3.5.3 Case Study Polypropylene – Nanoclay

Figure 3.5.3.1 Extrusion line at Addiplast SAS.

3.6 WP6 Standardisation and technology evaluation

3.6.1 Main objectives

3.6.2 Economic and ecological evaluation

3.6.3 Standardisation

4. Description of potential impact, dissemination activities and exploitation of results

Key exploitable results in NanoOnSpect			
Nr.	**Key exploitable results**	**Exploitation manager**	
1	**^{on}BOX characterisation device**	**Gneuss**	
2	**Nanocomposite compounding**	**Nexxus**	
3	**Intelligent Module for nanocomound processing**	**Ateknea**	
Exploitable Results			**Input for Key exploitable result Nr.**
1	Sensor for Microwave	**HBH/FhG-ICT**	**1**
2	Knowledge on microwave spectroscopy -	**HBH/FhG-ICT**	**1**
3	Sensor for thermal conductivity	**Hukseflux**	**1**
4	Knowledge on optical spectroscopy	**FhG-ICT**	**1**
5	Knowledge on Raman spectroscopy	**FhG-ICT**	**1**
6	Sensor for ultrasonic spectroscopy	**Ateknea**	**1**
7	Sensor for nanocompound rheology	**Gneuss**	**1**
8	Optical multi-spot temperature sensor	**FOS**	**1**
9	Sensors for pressure	**FOS**	**1**
10	Knowledge on nanocompound processing	**AIMPLAS/FhG-ICT/Nexxus/Colorex/Addiplast**	**2**
11	Nexxus channel technology for nanocompound processing	**Nexxus**	**2**
12	Knowledge on nanocompound characterisation	**AIMPLAS/FhG-ICT/Nexxus/Colorex/Addiplast**	**1/2/3**

Figure 4.3.1 List of exploitable results of the project

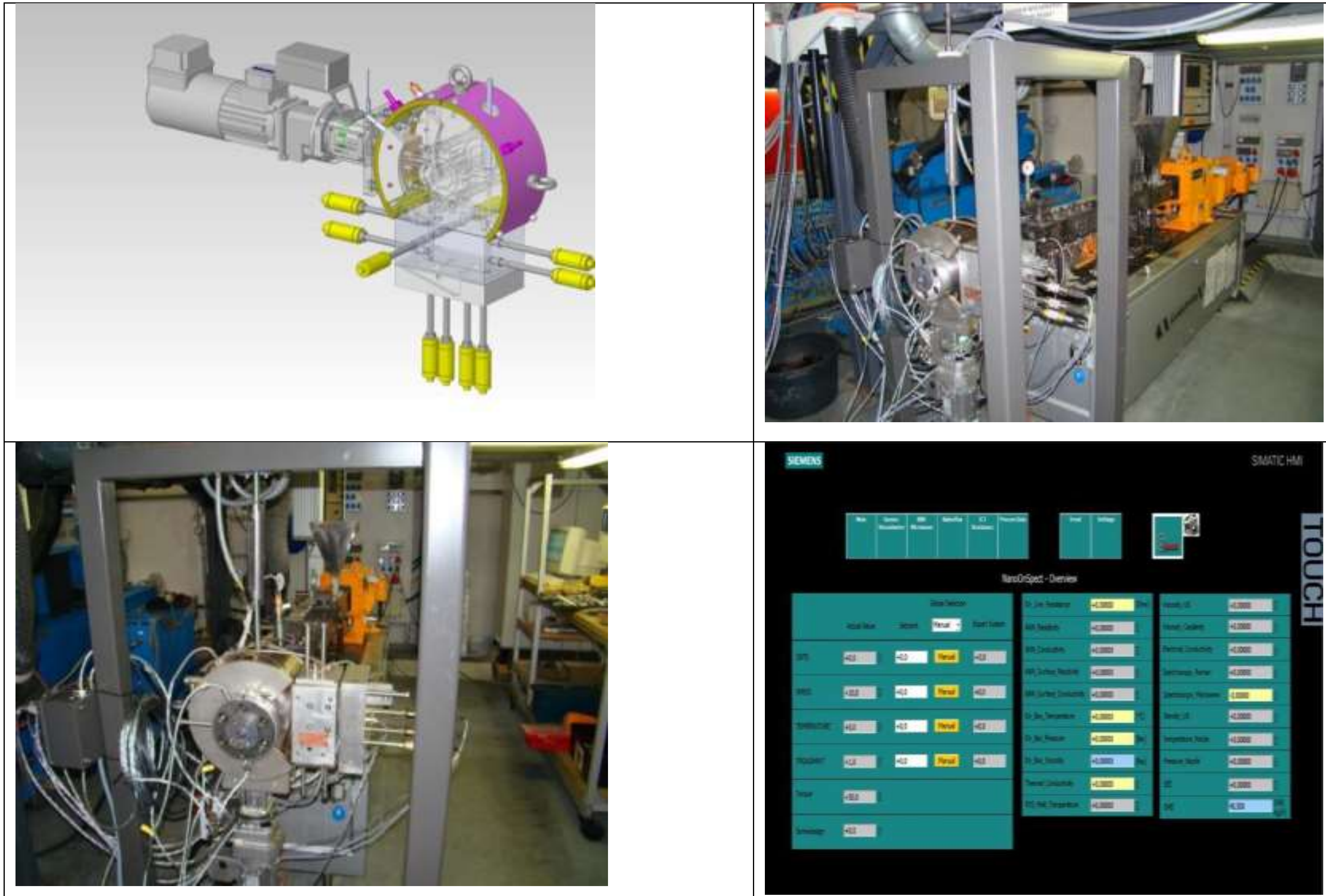

Figure 4.3.2: ^{on}BOX and it's controller

Short description of the Nexxus channel

Figure 4.3.2: 1. Nexxus Melting NXBG200W80 ME, 2. Pumping group for the slurry, 3. Nexxus Degassing NXBG200W80 DE